THE EFFECT OF BFPP MUTATIONS ON TRAFFICKING, SIGNALING AND FUNCTION OF ADGRG1/GPR56 RECEPTOR

A THESIS SUBMITTED TO
THE GRADUATE SCHOOL OF NATURAL AND APPLIED SCIENCES
OF
MIDDLE EAST TECHNICAL UNIVERSITY

BY

NİL DEMİR

IN PARTIAL FULFILLMENT OF THE REQUIREMENTS
FOR
THE DEGREE OF MASTER OF SCIENCE
IN
BIOLOGY

SEPTEMBER 2022

Approval of the thesis:

THE EFFECT OF BFPP MUTATIONS ON TRAFFICKING, SIGNALING AND FUNCTION OF ADGRG1/GPR56 RECEPTOR

submitted by **NİL DEMİR** in partial fulfillment of the requirements for the degree of **Master of Science** i**n Biology, Middle East Technical University** by,

Prof. Dr. Halil Kalıpçılar
Dean, Graduate School of **Natural and Applied Sciences** _____

Prof. Dr. Ayşe Gül Gözen
Head of the Department, **Biological Sciences** _____

Assoc. Prof. Dr. Çağdaş Devrim Son
Supervisor, **Biological Sciences, METU** _____

Dr. Orkun Cevheroğlu
Co-Supervisor, **Stem Cell Institute, Ankara University** _____

Examining Committee Members:

Prof. Dr. Sreeparna Benarjee
Biological Sciences, METU _____

Assoc. Prof. Dr. Çağdaş Devrim Son
Biological Sciences, METU _____

Assoc. Prof. Dr. Pınar Baydın
Stem Cell Institute, Ankara University _____

Date: 12.09.2022

I hereby declare that all information in this document has been obtained and presented in accordance with academic rules and ethical conduct. I also declare that, as required by these rules and conduct, I have fully cited and referenced all material and results that are not original to this work.

Name Last name :

Signature :

ABSTRACT

THE EFFECT OF BFPP MUTATIONS ON TRAFFICKING, SIGNALING AND FUNCTION OF ADGRG1/GPR56 RECEPTOR

Demir, Nil
Master of Science, Biology
Supervisor: Assoc. Prof. Dr. Çağdaş Devrim Son
Co-Supervisor: Dr. Orkun Cevheroğlu

September 2022, 61 pages

Bilateral frontoparietal polymicrogyria (BFPP) is a hereditary brain abnormality characterized by defects on the brain cortex surface in the form of smaller (micro-) and multiplexed (poly-) gyri and sulci. More than 20 mutations in the ADGRG1/GPR56 gene have contributed to BFPP in various clinical studies, including in Turkish patients. ADGRG1/GPR56 receptor belongs to the adhesion G protein-coupled receptor family (aGPCR). Even though some of these mutations were found to reduce cell surface expression of the receptor, structural properties and molecular mechanisms of BFPP mutations that affect ADGRG1/GPR56 function are yet unknown. The study aims to (*i*) visualize the cell surface expression of tagged ADGRG1/GPR56 receptors carrying BFPP mutations using a laser scanning confocal microscope, (*ii*) investigate the effects of BFPP mutations on the receptor and Gα12 interactions, and (*iii*) investigate the effects of BFPP mutations on the receptor and β-arrestin interactions using Bioluminescence Resonance Energy Transfer (BRET) biosensors in live cells. Herein, eight missense BFPP mutations were introduced on ADGRG1/GPR56 receptor by using site-directed mutagenesis.

The results showed mutant receptors had decreased cell surface expression compared to the wild-type. Gβ/ɣ and GRK, based BRET biosensors were used to investigate the coupling of ADGRG1/GPR56 with Gα12. C346S, W349S, and L640R mutations decreased the interaction of the receptor with Gα12 with respect to the wild-type. Arrestin-based BRET biosensor was used to investigate β-arrestin recruitment following receptor activation. All mutations tested in this study showed decreased beta-arrestin recruitment to the plasma membrane compared to the wild-type.

Keywords: BFPP, BRET, GPR56, ADGRG1, Adhesion GPCR

ÖZ

BFPP MUTASYONLARININ ADGRG1/GPR56 RESEPTÖRÜNÜN TRAFİĞİ, SİNYALİZASYONU VE İŞLEVİ ÜZERİNDEKİ ETKİSİ

Demir, Nil
Yüksek Lisans, Biyoloji
Tez Yöneticisi: Doç. Dr. Çağdaş Devrim Son
Ortak Tez Yöneticisi: Dr. Orkun Cevheroğlu

Eylül 2022, 61 sayfa

İki Taraflı Frontoparietal Polimikrojiri, beyin korteks yüzeyinde normalden daha küçük (mikro) ve çok sayıda (poli-) girus ve sulkus şeklinde kusurlarla karakterize kalıtsal bir beyin anormalliğidir. ADGRG1/GPR56 genindeki 20'den fazla mutasyonun, Türk hastalar da dahil olmak üzere çeşitli klinik araştırmalarda BFPP geliştirdiği gösterilmiştir. ADGRG1/GPR56 reseptörü adezyon G proteinine kenetli reseptör ailesinin (aGPCR) bir üyesidir. Bu mutasyonların bazılarının reseptörün hücre yüzeyi ekspresyonunu azalttığı bulunmuş olsa da, ADGRG1/GPR56 fonksiyonunu etkileyen BFPP mutasyonlarının yapısal özellikleri ve moleküler mekanizmaları henüz bilinmemektedir. Çalışmanın amacı (*i*) BFPP mutasyonları taşıyan ADGRG1/GPR56 reseptörlerinin hücre yüzeyi ekspresyon profilini lazer taramalı konfokal mikroskop ile (*ii*) mutant reseptörler ile Gα12 arasındaki ve (*iii*) mutant reseptörler ile β-arrestin proteini arasındaki etkileşimleri Biyolüminesans Rezonans Enerji Transferi (BRET) temeline dayalı biyosensörler yolu ile canlı hücrelerde araştırmaktır. Bu bağlamda, sekiz farklı yanlış anlamlı mutasyon, bölgeye yönelik mutajenez yöntemi ile ADGRG1/GPR56 reseptörü üzerinde

oluşturulmuştur. Sonuçlar mutant reseptörlerin doğal fenotip ile karşılaştırıldığında, reseptörün hücre yüzeyi ekspresyonunu azalttığını göstermektedir. Gβ/ɣ ve GRK temelli BRET biyosensörleri, reseptörün Gα12 ile eşleşmesini araştırmak için kullanılmıştır. Sonuçlar C346S, W349S ve L640R mutasyonlarının, doğal fenotip ile karşılaştırıldığında, reseptörün Gα12 ile etkileşimini azalttığını göstermektedir. Arrestin temelli BRET biyosensörleri ise, reseptör aktivasyonu neticesinde beta-arrestin molekülünün hücre zarındaki birikimini araştırmak için kullanılmıştır. Sonuçlar, tüm BFPP mutantlarının, doğal fenotip reseptör ile karşılaştırıldığında beta-arrestin molekülünün hücre zarında birikimini azalttığını göstermektedir.

Anahtar Kelimeler: BFPP, BRET, GPR56, ADGRG1, Adhezyon GPCR

To my family, who unconditionally love and support me.

ACKNOWLEDGMENTS

I am grateful to my advisor, Assoc. Prof. Dr. Çağdaş Devrim Son and my co-advisor Dr. Orkun Cevheroğlu, beyond words for their guidance and support throughout my journey. Without their contribution and encouragement, this thesis would not have been. Over the years that I have worked under the advisory of Dr. Son, he was always willing to help with a huge smile and picked up every phone call from me (even if the number of calls reached dozens per day). Dr. Cevheroğlu taught me how to do science, collaborate, and be a professional, eventually becoming a supportive friend in addition to a good mentor. I am also grateful to Assoc. Prof. Dr. Pınar Baydın for her precious advice and sincere approach. Additionally, I owe Assoc. Prof. Dr. Salih Özçubukçu for this thesis because he produced the most crucial molecule in this work.

I will never forget my lab partner Merve Murat's support and kindness. She enlighted my journey with her patience, grace, and courtesy. It was a privilege to work with her. Berkay Demirbaş and Dilara Öğütçü were the ones who transformed our small team into a strong research team. Besides being wonderful friends in my personal life, they became the best colleagues ever. They became my hands when my hands shook, my prevision during my anxiety attacks, and more… I owe them my most sincere thanks. Very special thanks to our Jr. lab member Betül Yiyen for her indescribable support and help during emendation process of my thesis.

Thanks to my lovely friends Emre Balbaşı and Funda Zekiye Ardıç for their guidance and unconditional support. Very special thanks to Ülfet Burcu Cinli and Batuhan Öcal for being my source of energy from hundreds of kilometers away.

Last but not least, I owe "the" greatest thanks to my dear family: my father, Mehmet Demir, my mother, Diclehan Demir, my sister Dicle Demir Kavruklar and my niece, Azra Kavruklar. They are the driving force behind everything I do. Their boundless and unconditional faith, support, and love allowed me to focus on and live my dreams to be a scientist. This thesis was written via years of love, patience, care, and encouragement from these beautiful people.

This work was partially funded by Scientific and Technological Research Council of Turkey under grant number TUBİTAK 118Z694.

TABLE OF CONTENTS

LIST OF TABLES

TABLES

LIST OF FIGURES

FIGURES

CHAPTER 1

INTRODUCTION

1.1 G Protein Coupled Receptors

Since their discovery, followed by intense classification studies, the biggest and most diverse class of cell surface receptors are guanine nucleotide-binding protein (G-protein)-coupled receptors (GPCRs) (Hill, 2006). In eukaryotes, they operate an evolutionarily conserved mechanism to perceive extracellular signals (Pierce, Premont, & Lefkowitz, 2002). The activation of intracellular signaling cascades by G-proteins mediated by a variety of agonists and ligands, including neurotransmitters, odorants, photons, cytokines, hormones, and even mechanical stimuli (Sanders, Brian, & Maze, 2008). Moreover, most biological processes incorporate GPCRs, making them the primary therapeutic target for numerous pathologies, like diabetes, hypertension, cardiovascular disease, and drug dependence (Hauser et al., 2018). Therefore, around 40% of all prescribed medicines target GPCRs (GPCRdb, 2022, June 23) and put these receptors in the spotlight for clinicians, academic researchers, and pharmaceutical manufacturers.

1.2 Molecular Organization and Activation of G Protein Coupled Receptors

With their plasma membrane anchored seven transmembrane helices (7-TM), three intracellular, and three extracellular loops, GPCRs constitute the largest family of integral membrane proteins. They feature a cytosolic C-terminal domain penetrating the surface of the cytosolic membrane and an N-terminal domain that is located on the outer surface of the cell membrane (Stenkamp, Teller, & Palczewski, 2002).

Interacting with a ligand result in a conformational change on GPCR leading to an active state to couple with heterotrimeric G proteins, GPCR kinases (GRK) and arrestins (Kobilka, 2007; Lefkowitz, 2000). In the G protein-dependent activation mechanism, ligand binding promotes the replacement of GDP attached to Gα subunit with GTP. Since GTP-bound Gα dissociates from Gβγ, both Gα and Gβγ subunits separately regulate intracellular downstream signaling processes (Duc, Kim, & Chung, 2015). GPCRs can also signal through arrestin proteins, which are thought to be actors in switching off the G protein signaling (Kuhn, 1978; Kuhn, Hall, & Wilden, 1984; Pfister et al., 1985). In addition, upon ligand binding, the C-terminal of the receptor is phosphorylated by GRKs, leading to arrestin recruitment. Subsequently, this precludes G protein interaction, facilitating receptor internalization (Kuhn, 1978; Kuhn et al., 1984).

1.3 Classification of G Protein Coupled Receptors

Formerly, GPCRs were classified upon their structural and physiological characteristics. However, after the Human Genome Project, the classification of GPCRs was shaped around genetic information. Upon intense phylogenetic analyses, GPCRs were classified into five fundamental families named as GRAFS: **G**lutamate, **R**hodopsin, **A**dhesion, **F**rizzled/Taste2, and **S**ecretin (Fredriksson, Lagerstrom, Lundin, & Schioth, 2003).

1.4 Adhesion G Protein Coupled Receptors

Adhesion GPCRs (aGPCRs) are one of the GPCR families with unique physical characteristics in addition to their riveting functional properties. With 33 members in humans (Fredriksson, Gloriam, Hoglund, Lagerstrom, & Schioth, 2003), aGPCRs are evolutionary conserved and ancient proteins that are found in many organisms from single-celled eukaryotes to most animals (Schioth, Nordstrom, & Fredriksson, 2010). Intriguingly, it is reported that aGPCRs have various splice variants which is

uncommon in most other GPCR families (Bjarnadottir et al., 2007). These splice variants lead to greater structural and functional variation in aGPCRs, which may have an impact on signaling pathways in the majority of human tissues (Knierim et al., 2019).

1.5 Biological Characteristics of Adhesion G Protein Coupled Receptors

1.5.1 Classification

aGPCRs were classified into nine different groups according to their specific domains on extracellular N-terminus and DNA sequence similarity corresponding to the seven-transmembrane domain. Except for ADGRA1/GPR123, all aGPCRs possess a unique **G**PCR **A**utoproteolysis **IN**ducing (GAIN) domain (Arac *et al*., 2012), which can be considered as a signature for this family. This specific domain contains **G**PCR **P**roteolysis **S**ite (GPS) motif, where the receptor splits into two and stays non-covalently bound as C-terminus and N-terminus heterodimer (Langenhan, Aust, & Hamann, 2013). As shown in Figure 1.1, each group has different ectodomains giving them functional variety.

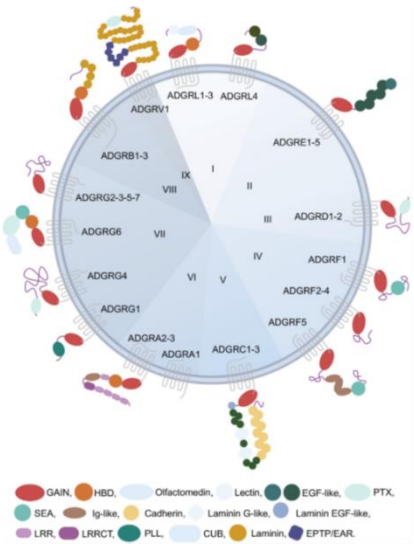

Figure 1.1 Nine groups of aGPCRs. Each ectodomain is showed in different shapes and colors. Taken from (Liebscher et al., 2021).

1.5.2 Structure

As in other GPCR families, aGPCRs have extracellular N-terminus, membrane-anchored seven-transmembrane domains, and an intracellular C-terminus. Uniquely, their extracellular N-terminal is much larger and contains various domains besides the aGPCR specific GAIN domain compared to other GPCRs (Liebscher et al., 2021). GAIN domain consists of A and B subunits. A subunit associates with N-terminus, while B subunit associates with the seven transmembrane domain of the receptor. B subunit also has a conserved sequence called the GPS motif, where autoproteolysis occurs and allows separation of the B subunit into B_N (N-terminus of B subunit) and B_C (C-terminus of B subunit). Depending on these features, there are two different classifications of aGPCRs: topology-based and cleavage-based (Figure 1.2). Topology-based compartmentation divides the receptor into three sections as extracellular (1), transmembrane (2), and intracellular (3). In contrast, cleavage-based compartmentation divides the receptor into two sections: N-terminal (I) and C-terminal (II) fragments. Accordingly, N-terminal fragment consists of A_N and B_N subunits of GAIN domain besides N-terminal domain of the whole receptor, while C-terminal fragment consists of B_C subunit of GAIN domain besides transmembrane and C-terminal domain of the whole receptor (Langenhan et al., 2013).

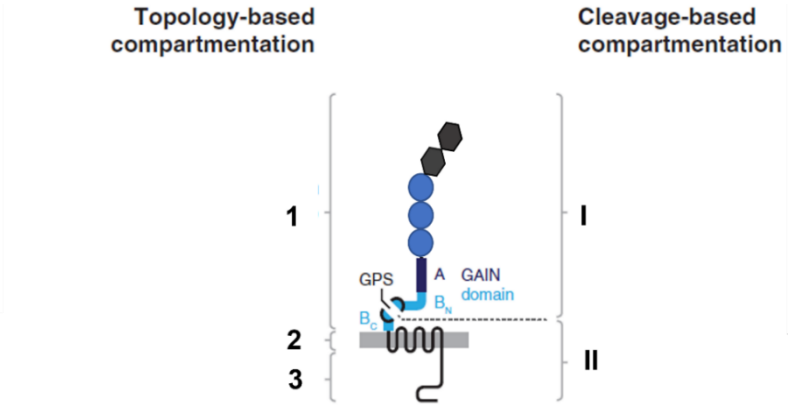

Figure 1.2 Structural compartmentalization of aGPCRs. Left hand side shows topology-based compartmentation. Right hand side shows cleavage-based compartmentation. Adapted from (Langenhan et al., 2013).

1.5.3 Function

Functional variety within aGPCRs is mediated by extremely varied N-terminal domains. Highly diverse adhesion domains on this structure may also have an important contribution to the functional variety among aGPCRs (Langenhan et al., 2013). ADGRG1/GPR56 has been associated with bilateral frontoparietal polymicrogyria (BFPP), which is a severe brain abnormality caused by a number of mutations in the GPR56/ADGRG1 gene (Piao et al., 2005). ADGRE5/CD97 is known for its role in the activation of leukocytes (Hamann et al., 1995). Additionally, it has a significant impact on adherens junctions, which affects the ability of intestinal epithelial cells to serve as barriers (Becker et al., 2010). Recent studies indicate that the recognition of pathogens is facilitated by ADGRE1/EMR1 in macrophages (Waddell et al., 2018). ADGRE2/EMR2 modulates systemic inflammation via elevating the activation of neutrophiles (Yona et al., 2008). ADGRG3/GPR97 is also involved in neutrophiles' antimicrobial activation (Hsiao et al., 2018). ADGRF5/GPR116 plays a crucial role in the homeostasis of pulmonary surfactants (Bridges et al., 2013). ADGRF1/GPR110 is involved in neuron development as well as spatial memory and recognizing objects (Lee et al., 2016). ADGRC1/CELSR1 has a specific role in brain development and is mostly engaged with planar cell polarity (L. Wang et al., 2018). ADGRC3/CELSR3 also plays a role in planar cell polarity via controlling axonal guidance (Lindenmaier, Parmentier, Guo, Tissir, & Wright, 2019). In peripheral nerves, especially during nerve healing (Mogha et al., 2016), ADGRG6/GPR126 plays a role in the development of myelin by Schwann cells (Monk, Oshima, Jors, Heller, & Talbot, 2011). In addition to being present in endothelial cells, ADGRL4/ELTD1 also functions as a pro-angiogenic factor. Besides, it is highly expressed in tumors and correlated with vascular maturation (Favara, Banham, & Harris, 2014). ADGRB1/BAI1 inhibits angiogenesis in the brain (Kaur, Brat, Devi, & Van Meir, 2005).

1.5.4 Activation

aGPCRs simply have four different receptor activation models: basal state, orthosteric (tethered-peptide) agonism, allosteric activation, and allosteric inhibition (Kishore, Purcell, Nassiri-Toosi, & Hall, 2016; Salzman et al., 2017; Stoveken, Hajduczok, Xu, & Tall, 2015; Vizurraga, Adhikari, Yeung, Yu, & Tall, 2020; Zhu et al., 2019). Depending on the unique properties of each receptor, aGPCRs display varying levels of basal activity. Many aGPCRs exhibit basal activity in the absence of ligands, which activates G proteins. This was explained by the fact that certain receptor molecules randomly assume an active conformation (Milligan, 2003). Another model of receptor activation called orthosteric agonism relies on the aGPCR tethered agonist activity. The seven residues next to the C-terminus of GPS domain are the most crucial ones and make the frame of the tethered agonist. The consensus sequence for these residues is TXFAVLM which overlaps with β-strand 13, and T, F, M amino acids are the most conserved among all aGPCRs (Vizurraga et al., 2020). *Stachel* sequence peptides, which are generated from this area, can activate the relevant receptor (Demberg et al., 2017). The orthosteric agonism model postulates that effective GAIN domain cleavage, followed by separation of the N-terminal fragment from C-terminal fragment, is necessary for signaling action (Zhu et al., 2019). However, another study shows that, G-protein mediated signaling is still possible with engineered receptors incapable of cleavage via autoproteolysis (Kishore & Hall, 2017). Overall, tethered agonist activation is highly complex and still needs to be understood. Allosteric activation and inhibition models postulate that ligand binding causes a conformational change in the receptor structure without dissociating its N-terminal and C-terminal fragments. Thus, the conformational change leads to the activation or inhibition of downregulated signaling pathways (Vizurraga et al., 2020).

1.6 Diseases Related to Adhesion G Protein Coupled Receptors

The physiological significance of the aGPCR family is revealed by the expression of aGPCRs in many different parts of the human body, including the central nervous system, immune system, reproductive organs, and kidneys, as well as by the direct relationship between these receptors and development (Liebscher et al., 2021). So far, three aGPCRs have been linked to monogenetic diseases. ADGRG1/GPR56 monogenetically causes bilateral frontoparietal polymicrogyria (BFPP) (Piao et al., 2005). ADGRV1/VLGR1 is found to be involved in type II Usher syndrome (Weston, Luijendijk, Humphrey, Moller, & Kimberling, 2004). It is reported that autosomal dominant vibratory urticaria patients carry an ADGRE2/EMR2 variant (Boyden, Desai, et al., 2016; Boyden, Metcalfe, & Komarow, 2016). ADGRL3/LPHN3 variants have been associated to attention deficit hyperactivity disorder (ADHD) (Arcos-Burgos & Muenke, 2010). Preclinical studies and human genetics demonstrate associations between aGPCRs and cancer (Gad & Balenga, 2020). Molecular impact of ADGRG1/GPR56 (Chiang *et al*., 2017; Xu, Begum, Hearn, & Hynes, 2006; Yang *et al.*, 2011), ADGRA2/GPR124 (Cherry *et al.*, 2019), ADGRA3/GPR125 (Y. Wu *et al.*, 2018), ADGRB1/BAI1 (D. Zhu & Van Meir, 2016), ADGRE5/CD97 (Li *et al*., 2015), and ADGRF5/GPR116 (Tang *et al*., 2013) in carcinogenesis is well understood. On the other hand, ADGRL/LPHN (Meza-Aguilar & Boucard, 2014), ADGRD1/GPR133 (Bayin et al., 2016) and ADGRV/VLGR1 (Y. Wang et al., 2015) are involved in cancer through the change in expression pattern or receptor activity.

1.7 Overview of ADGRG1/GPR56

Human ADGRG1/GPR56 gene is located on chromosome 16q21 and covers about 45 kb of DNA. It has 14 exons and a coding region that is 2082 bp long from exon 2 to exon 14. Various tissue types express this receptor, such as thyroid glands, skeletal muscles, testicles, kidneys, pancreas, and brain (Liu et al., 1999). Accordingly, it

plays various roles in muscle hypertrophy, neural and hematopoietic stem and progenitor cell maintenance, stress and depression, synaptic remodeling in the central nervous system, and cytotoxic lymphocytes steady state (Singh & Lin, 2021). ADGRG1/GPR56 possesses four different proteins resulting from alternative RNA splicing (Bjarnadottir et al., 2007; Salzman et al., 2016), and the first non-coding exon contains 17 different translation initiation sites. Each of them has unique expression patterns in humans. The PLL (Pentraxin/Laminin/neurexin sex-hormone binding globulin-Like) and GAIN domains are two distinct protein domains found in the extracellular region of ADGRG1/GPR56. The PLL domain is specific to ADGRG1/GPR56, which weakens the basal activity of the receptor. Autoproteolysis takes place between Leu-382 and Thr-383 at the GPS domain, which is a part of the GAIN domain (Singh & Lin, 2021). ADGRG1/GPR56 receptor can be activated by numerous mechanisms: autoproteolysis dependent (Zhu et al., 2019), autoproteolysis independent (Kishore & Hall, 2017), tethered peptide agonist dependent (Stoveken et al., 2015), and tethered peptide agonist independent (Salzman et al., 2017). Transglutaminase 2 (TG2) (Xu, Begum, Hearn, & Hynes, 2006) and collagen III (Col3A1) (Luo et al., 2011) are known ligands that activate ADGRG1/GPR56. In response to interaction with the tetraspanins CD9 and CD81, it is shown that ADGRG1/GPR56 couples to Gαq/11 (Little, Hemler, & Stipp, 2004). In response to ligand binding, ADGRG1/GPR56 also couples to the Gα12/13 and activates the RhoA and mTOR pathways (Ackerman, Garcia, Piao, Gutmann, & Monk, 2015; Iguchi et al., 2008; Luo et al., 2011; White et al., 2014).

1.8 Bilateral Frontoparietal Polymicrogyria

A cortical malformation known as polymicrogyria, an autosomal recessively inherited condition, is characterized by improper cortical lamination and excess number of small gyri (Piao et al., 2005). The BFPP gene is located on chromosome 16q12–21 (Piao et al., 2002). There are 11 different identified mutations involved in BFPP patients. One of them is a deletion mutation that results in frameshift through

translation and termination of proteins without being matured. Two of them are splicing mutations located on Intron 9. Last eight of them are missense mutations located on GPR56 gene 16q21. Four of these eight mutations (R38Q, R38W, Y88C, C91S) present on N-terminal region; two of them (C346S, W349S) are located on GPS domain; one of them (R565W) is at the second extracellular loop, and the last one is at the third extracellular loop of GPR56 protein (Piao et al., 2005). ADGRG1/GPR56 is known to mediate cell-cell and cell-matrix interactions, thereby controlling various aspects of brain development in a cell type specific manner (Langenhan, Piao, & Monk, 2016; Singer, Luo, Jeong, & Piao, 2013). During embryonic brain development, ADGRG1/GPR56 has been shown to be expressed in neural progenitor cells and migrating nerve cells and interact with an extracellular matrix protein, Col3A1, to regulate cortical lamination by activating the Rho signaling pathway via Gα12/13 (Jeong, Luo, Li, Strokes, & Piao, 2012; Luo et al., 2011). Various studies have shown that ADGRG1/GPR56 is highly expressed in astrocytes, oligodendrocyte cell lines and microglia from glial cells during the later stages of brain development and postnatal life (Bennett et al., 2016; Zhang et al., 2014). In addition to these studies, ADGRG1/GPR56 is shown to control developmental myelination and myelin repair via the Gα12/13–Rho signaling pathway by interacting with TG2, a ligand produced by microglia, and laminin, an extracellular matrix protein, in oligodendrocyte precursor cells (Ackerman et al., 2015; Giera et al., 2015; Giera et al., 2018). ADGRG1/GPR56 expressed in Schwann cells in the peripheral nervous system (PNS), interacts with Plectin, a large cytoskeleton-binding protein, activating the Gα12/13-Rho signaling pathway and remodeling the cytoskeleton, which plays a role in myelination of PNS neurons (Ackerman et al., 2018). ADGRG1/GPR56 positively regulates cell proliferation in oligodendrocyte progenitor cells (OPC), and negatively regulates differentiation of OPCs into oligodendrocytes. It is also shown that ADGRG1/GPR56 colocalizes with α3β1 integrin, which binds to laminin-511 in radial glial cells and rostal prepalte neurons (Jeong et al., 2013). This coupling indicates that the α3β1 integrin regulates cortical development in coordination with ADGRG1/GPR56. A recent study has

shown that an ADGRG1/GPR56 splice isoform is required for microglia-mediated synapse healing by binding to phosphatidylserine via the GAIN domain (Li et al., 2020). In addition to defining the microglial cell type, ADGRG1/GPR56 is one of the few genes whose expression requires appropriate ontogeny and environmental influences. To summarize, ADGRG1/GPR56 shows brain cortical pattern and healthy development of the cerebral cortex, rostral cerebellar development, neuron axon myelination and myelin repair in both the CNS and PNS, OPC proliferation, inhibition of OPC differentiation in the CNS to oligodendrocytes, and proper radial sorting in Schwann cells.

1.9 Bioluminescence Resonance Energy Transfer (BRET)

Bioluminescence energy transfer (BRET) is a biophysics tool to investigate protein-protein interactions, and its theory is based on non-radiative resonance energy transfer between a bioluminescent donor molecule and a fluorescent acceptor molecule. In this method, the bioluminescent donor molecule is activated by its substrate. This activation is achieved by oxidation of the substrate by the bioluminescent enzyme (donor). The energy produced by this reaction results in bioluminescent photon emission. If there is an acceptor molecule nearby (less than 10 nm) bioluminescent molecule could transfer part of its energy non-radiatively to the accepter instead of emitting a photon. Then, transferred energy excites the acceptor molecule if its excitation spectrum overlaps with the bioluminescence spectrum of the donor. Thus, the excited acceptor can now emit a photon if it is a fluorescent molecule. Therefore, resonance energy transfer can be calculated by the ratio of light emitted by the acceptor to the donor (Kobayashi & Bouvier, 2021; Wu & Brand, 1994).

1.10 BRET Biosensors

BRET is an effective technique for shedding light on the dynamics of protein-protein interactions between GPCRs, G proteins, β-arrestins, and their various other binding partners. In this technique, one protein of interest will be tagged with a bioluminescent donor, and the other one will be tagged with a fluorescent acceptor. This traditional method modifies the protein by tagging, thus may change the normal signaling of the protein of interest, especially GPCRs. In order to overcome this obstacle, G protein biosensors based on BRET were constructed over the last decade (Donthamsetti, Quejada, Javitch, Gurevich, & Lambert, 2015; Gales et al., 2006; Masuho, Skamangas, & Martemyanov, 2020; Salahpour et al., 2012; Schihada, Shekhani, & Schulte, 2021; Yano et al., 2017).

1.10.1 GRK and Gβɣ mediated BRET sensors

The coupling between GPCRs and Gα12 protein mediated by GRK can be measured using biosensors based on resonance energy transfer and without the necessity of tagging the receptor (Masuho et al., 2020). Using untagged receptors is advantageous because it eliminates the possible interaction problems between GPCR and Gα12 protein caused by tagging. As shown in Figure 1.3, these sensors are constructed by tagging Gɣ with the first 155 amino acids of Venus, Gβ with 156-239 amino acids of Venus, and GRK with NLuc. In the inactive state of the receptor, the Gα and Gβ/Gγ subunits form a heterotrimeric structure and do not interact with the membrane-localized GRK3 protein. Therefore, low BRET values are measured in the inactive state of the receptor. In the active state of the receptor, the Gβ/Gγ subunits separate from Gα, and approach the GRK3 protein, and higher BRET values are measured. Herein, BRET occurs between the donor NLuc and the acceptor Venus. Thus, receptor-G protein interactions can be measured in this way. The reason for using split Venus for tagging Gβγ instead of just tagging Gβ or Gγ with intact Venus is to show tagging did not prevent Gβ/Gγ coupling.

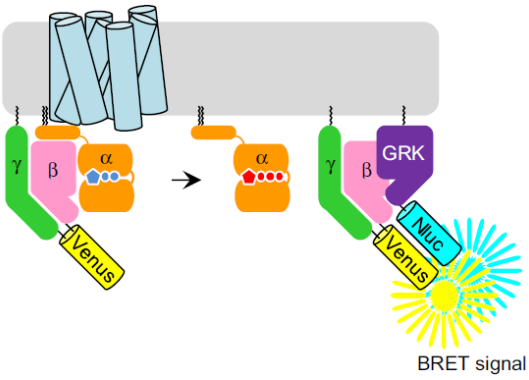

Figure 1.3 Illustration showing the working principle of Gβ/ɣ and GRK mediated BRET sensors. Taken from (Masuho et al., 2020).

1.10.2 Arrestin-mediated BRET sensors

Recruitment of beta-arrestin to the cell membrane can be measured by using beta-arrestin mediated BRET sensors (Donthamsetti et al., 2015). As shown in Figure 1.4, these sensors are constructed by tagging arrestin with bioluminescent protein Rluc8 and tagging GAP43 with fluorescent protein citrine. In the inactive state of the receptor, beta arrestin is not recruited to the plasma membrane and does not interact with membrane marker GAP43. Therefore, low BRET values are measured in the inactive state of the receptor. In the active state of the receptor, beta-arrestin is recruited to the receptor located on the cell membrane. This increases the bystander BRET between beta-arrestin and membrane protein GAP43 due to random proximity. Therefore, higher BRET values are measured.

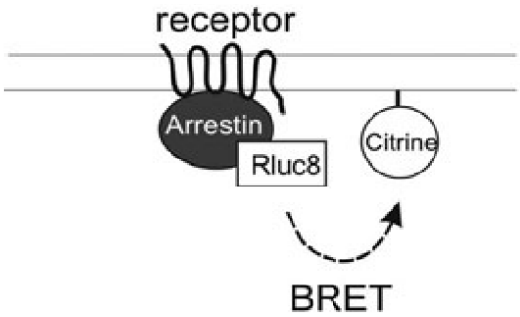

Figure 1.4 Illustration showing the working principle of beta-arrestin mediated BRET sensors. Taken from (Donthamsetti et al., 2015).

1.11 Aim of the Thesis

This thesis aims to investigate the effects of BFPP mutations on ADGRG1/GPR56 receptor trafficking using EGFP tagged receptor constructs and imaging them with Laser Scanning Confocal Microscopy; and to investigate the effects of BFPP mutations on the receptor signaling by measuring the coupling with Gα and beta-arrestin using BRET based biosensors.

CHAPTER 2

MATERIALS AND METHODS

2.1 Construction of EGFP Tagged ADGRG1/GPR56

The plasmid contains human ADGRG1/GPR56 receptor cDNA is a kind gift from Assoc. Prof. Dr. Demet Araç (University of Chicago). pEGFP-N1, a plasmid containing EGFP cDNA, was used to construct cassettes with linker sequence (Gly-Ser-Ser-Gly) in pcDNA3.1+, which will be referred to as "L" throughout the text. Construction of L-EGFP tagged ADGRG1/GPR56 with the linker was done using the insertional PCR method. This method consists of two consecutive PCRs. First-PCR aims to amplify L-EGFP by using a primer pair containing its 5' and 3' homologous L-EGFP sequences and flanking sequences homologous to C-terminus of ADGRG1/GPR56. The product from the first-PCR was used in second-PCR as a tandem primer to fuse L-EGFP with ADGRG1/GPR56 in pcDNA 3.1+, using high fidelity DNA polymerase. Primer pair for first-PCR was shown in Table 2.1; components and reaction conditions were shown in Table 2.2.

Table 2.1 Sequences of primers used first PCR.

Primer	**Sequence**
AG1-Ct-L-E-F	5' cccatcagctcgggcagcacctcgtccagccgcatcGGCAGCAGCGGCGTGAGCAAGGGC 3'
AG1-Ct-L-E-R	5' cagcgggtttaaacgggccctctagactcgagcctaCTTGTACAGCTCGTCCATGCCG 3'

Table 2.2 Components and reaction conditions of first PCR.

Component	Volume in µL	Final Concentration in 20 µL
pEGFP-N1 plasmid	x	100 ng
AG1-Ct-L-E-F	0.5	0.5 µM
AG1-Ct-L-E-R	0.5	0.5 µM
Nuclease Free Water	12.6-x	
5x Phire High Fidelity Buffer	4	1x
Phire Hot Start II DNA Polymerase	0.4	0.02 U/ µL
2 mM dNTPs	2	200 µM of each

98°C	30s	
98°C	**10s**	
54°C	**30s**	**x35 cycle**
72°C	**15-30s s/kb**	
72°C	60s	

Purification of first-PCR was done by using Thermo Scientific™ GeneJET Purification Kit, as recommended by the manufacturer. The purified product of the first-PCR was used in the second-PCR as a primer. The molar ratio of the first-PCR product and template plasmid (ADGRG1/GPR56 in pcDNA 3.1+) is 1:20. Components and reaction conditions of the second-PCR is shown in Table 2.3.

Table 2.3 Components and reaction conditions of second PCR.

Component	Volume in µL	Final Concentration in 20 µL
ADGRG1/GPR56 in pcDNA 3.1+	x	200 ng
Fist PCR Product	y	
Q5 High Fidelity DNA Polymerase	0.2	0.02 U/ µL
5x Q5 Reaction Buffer	4	1x
5x Q5 High GC Enhancer	4	1x
Nuclease Free Water	9.8-(x+y)	
2 mM dNTPs	2	200 µM of each

98°C	30s	
98°C	**10s**	
54°C	**30s**	**x35 cycle**
72°C	**30s s/kb**	
72°C	120s	

Afterward, second-PCR reaction mixture was treated with Fast Digest DpnI (Thermo Scientific™, USA) restriction enzyme, as recommended by the manufacturer. In this reaction, DpnI enzyme digests methylated parental template DNA (ADGRG1/GPR56 in pcDNA 3.1+). As a result, the newly synthesized L-EGFP tagged ADGRG1/GPR56 pcDNA 3.1+ plasmid remains in the PCR tube. For isolating the constructed plasmids, competent DH5α *E. coli* cells were transformed using the DpnI treated PCR mixture. Accordingly, 50 µL of competent cells were mixed with 2 µL of the reaction mixture under aseptic conditions, followed by incubation for 30 minutes on ice. Afterward, cells were heat shocked for 45 seconds at 42°C and, immediately after, incubated for 5 minutes on ice again. Then, cells were mixed with 950 µL of Super Optimal Broth with catabolite repression and incubated for 1 hour at 37°C and 330 rpm with constant shaking. Afterward, cells were centrifuged for 3 minutes at 6000 rpm, and 800 µL of supernatant was removed. Cell pellets were resuspended with the remaining 200 µL supernatant. Since pcDNA 3.1+ has Ampicillin resistance, transformed cells were seeded onto agar plates containing ampicillin and incubated overnight at 37°C. Next day, colonies on the plate were picked up and seeded in Luria-Bertani broth containing ampicillin, followed by overnight incubation at 37°C and 330 rpm with constant shaking. Plasmids were isolated with Thermo Scientific™ GeneJET Plasmid Miniprep Kit as recommended by the manufacturer.

2.2 Induction of BFPP Mutations on ADGRG1/GPR56

Eight missense mutations, found in BFPP patients, were introduced to wild-type, and L-EGFP tagged ADGRG1/GPR56 by using site-directed mutagenesis with double primer method (Figure 2.1). This method based on amplifying the entire vector with both forward and reverse primers containing the bases that need to be changed at certain positions. Although the 5' ends of the primers overlap, the differences in the 3' ends allow the plasmid to be replicated efficiently by carrying the mutation of interest. Since the entire vector was amplified, Q5® High-Fidelity DNA Polymerase

(NEB, USA) with low error rate and high sensitivity was used in this reaction. Details about BFPP mutations and primers used in site-directed mutagenesis were given in Table 2.4; PCR components and conditions for site-directed mutagenesis was shown in Table 2.5.

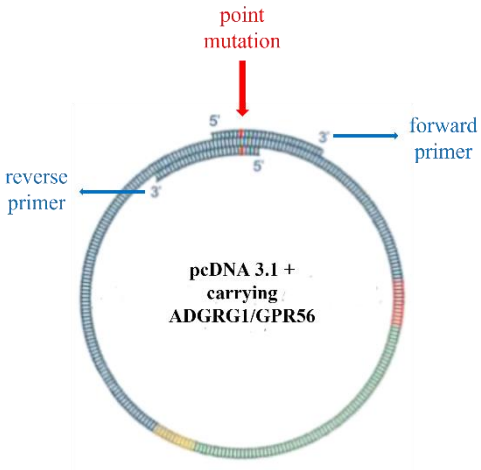

Figure 2.1 Schematic representation of site-directed mutagenesis method.

Table 2.4 BFPP mutations on ADGRG1/GPR56 and primers to induce these mutations.

Amino acid change	Base change	Primer	Sequence
R38W	112 C > T	G1-R38W-F	5' tgcagccag**t**ggaaccagacacacaggagc 3'
		G1-R38W-R	5' ctggttcc**a**ctggctgcagaagcgaaagtc 3'
Y88C	263 A > G	G1-Y88C-F	5’ aggggcctct**g**ccacttctgcctctactggaac 3’
		G1-Y88C-R	5’ gcagaagtgg**c**agaggcccctggggtcagg 3’
C91S	272 G > C	G1-C91S-F	5' ctctaccacttct**c**cctctactggaaccgacatgctggg 3'
		G1-C91S-R	5’ ccagtagaggg**g**agaagtggtagaggcccctggg 3’
C346S	1036 T > A	G1-C346S-F	5’ gactctgcaa**a**gtgtgttctgggttgaagacccc 3’
		G1-C346S-R	5' ccagaacacact**t**tgcagagtcacattcttcgg 3'
W349S	1046 G > C	G1-W349S-F	5' tgtgtgttct**c**ggttgaagaccccacattgagc 3'
		G1-W349S-R	5' gtcttcaacc**g**agaacacacattgcagagtcac 3'
R565W	1693 C > T	G1-R565W-F	5' gtgctggatc**t**gggactccctggtcagctac 3'
		G1-R565W-R	5' cagggagtccc**a**gatccagcacatggaagg 3'
L640R	1919 T > G	G1-L640R-F	5’ cttgtcgtcc**g**ctacctttcagcatcatcacc 3’
		G1-L640R-R	5’ gaaaaggtag**c**ggacgacaagctggaaggtgcc 3’

Table 2.5 Components and conditions of site-directed mutagenesis PCR to induce BFPP mutations on ADGRG1/GPR56.

Component	**Volume in µL**	**Final Concentration in 20 µL**
ADGRG1/GPR56 in pcDNA 3.1+	1	100 ng
20 µM Forward Primer	0.5	
20 µM Reverse Primer	0.5	
5x Q5 High Gc Enhancer	4	1x
5X Q5 Reaction Buffer	4	1x
Q5 High Fidelity DNA Polymerase	0.2	0.02 U/ µL
2 mM dNTPs	2	200 µM of each
Nuclease Free Water	7.8	

98°C	30s	
98°C	**10s**	**x35 cycle**
59°C	**30s**	
72°C	**5min**	
72°C	120s	

Plasmids carrying ADGRG1/GPR56 cDNA with BFPP mutations were verified with Sanger sequencing. Sequencing primers for each mutation was shown in Table 2.6. Sequencing results were analyzed by using Basic Local Alignment Search Tool (BLAST).

Table 2.6 Sequencing primers to detect BFPP mutations on ADGRG1/GPR56.

Mutation	**Primer**	**Sequence**
R38W	seqp31-1f	GTGTACGGTGGGAGGTCTAT
Y88C		
C91S		
C346S	h56_GAIN_BH3_GR	CCGAGGAGACCATCAGCACTGCAAAG
W349S		
R565W	h56S1p2_3.1GF	CAGGAGGAAACCTCGGGACTAC
L640R	seqp31-1r	AGGAAAGGACAGTGGGAGTG

2.3 Cell Culture

2.3.1 Maintenance of HEK293 cell line

Complete growth medium for HEK293 cells was prepared by using Dulbecco's Modified Eagle Medium (90 %) (ThermoFisher Scientific, USA); Fetal Bovine Serum (10 %) (ThermoFisher Scientific, USA), and Penicillin/Streptomycin (1 %) (ThermoFisher Scientific, USA). Cells were grown in T25 cell culture flask under humidified atmosphere conditions containing 5 % CO_2 at 37°C. Cells were maintained under aseptic conditions in laminar flow, and all reagents used in cell culture procedures were stored in sterile conditions. When 1 x 10^6 HEK293 cells were seeded in T25 cell culture flask, these cells reached ~90 % confluency in three days. Hence, cells were sub-cultured twice a week. On the sub-culture day, the growth medium was removed, and cells were washed with pre-warmed 1x Dulbecco's Phosphate Buffered Saline, (Biological Industries, Israel) and treated with 1x TrypLE™ (ThermoFisher Scientific, USA) to detach adherent cells from the surface of cell culture flask. When the cell monolayer was disappeared, the flask surface was washed with a complete growth medium, and detached cells were centrifuged at 900 rpm for 5 minutes. Following that, the supernatant was removed, and the cell pellet was gently resuspended in a pre-warmed complete growth medium. Cells were counted by using hemocytometer under ZEISS Axio Vert.A1 inverted microscope (Zeiss, Germany), and 1 x 10^6 cells were seeded to a new T25 cell culture flask containing a pre-warmed fresh complete growth medium.

2.3.2 Transient transfection of HEK293 cells

Transient transfection of plasmid DNA was done by using Invitrogen™ Lipofectamine™ LTX Reagent with PLUS™ Reagent, as recommended by the manufacturer's protocol. Details about the transfection were shown in Table 2.7. When the confluency of seeded cells reached to ~85 %, the recommended amount

of PLUS Reagent and DNA was mixed within OptiMEM Reduced Serum Medium with phenol red (ThermoFisher Scientific, USA). Independently, the recommended amount of LTX was mixed with OptiMEM. LTX-OptiMEM mixture was added to PLUS-DNA-OptiMEM mixture and incubated for 30 minutes at room temperature. Following that, the growth medium on the cells was replaced with a pre-warmed fresh growth medium, and transfection reagent was gently added to it. Then, cells were incubated under humidified atmosphere conditions containing 5 % CO_2 for 24 hours at 37 °C.

Table 2.7 Cell numbers and amounts of reagents used in transient transfection of HEK293 cells in accordance with culture vessels.

Culture vessel	Cells per well	OptiMEM	DNA	PLUS	LTX
35 mm glass bottom	500000	100 µL	2500 ng	1 µL/1 µg DNA	5 µL/1 µg DNA
35 mm plastic dish	500000	100 µL	2500 ng	1 µL/1 µg DNA	5 µL/1 µg DNA
24 well plate	200000	50 µL	500 ng	1 µL/1 µg DNA	5 µL/1 µg DNA

2.4 Imaging with Laser Scanning Confocal Microscope

HEK293 cells were seeded on glass bottom culture dish and double-transfected with GAP43-mCherry as a plasma membrane marker and L-EGFP tagged ADGRG1/GPR56 plasmids. Cells were imaged using Zeiss LSM880 Laser Scanning Confocal Microscope. The objective used in imaging is 63x/1.4 Plan Apochrome Oil DIC. Excitation of EGFP and mCherry was performed by Argon laser (488nm for EGFP, 594 nm for mCherry), while emissions were measured at 493-586 nm for EGFP and 599-754 nm for mCherry.

2.5 Western Blot Analysis

2.5.1 Lysis and sample preparation

HEK293 cells were seeded on 35 mm plastic cell culture dish and transfected with wild-type and constructed ADGRG1/GPR56 plasmids. 24 hours after transfection, cells were transferred on ice, and all reagents and microcentrifuge tubes were meanwhile pre-chilled. The growth medium was removed, and cells were washed with 1x cold PBS. Following that, 500 µL of 1x Radioimmunoprecipitation (RIPA) buffer (see Appendix) was added to the cells. Cells were detached and lysed by a cell scraper and transferred to microcentrifuge tubes. Tubes were incubated for 30 minutes on ice and vortexed every 5 minutes during incubation. Then, cells were centrifuged at 4°C and 16000 x g for 20 minutes to remove the cell debris. The supernatant, containing the proteins, was carefully transferred to new microcentrifuge tubes. Protein concentrations were measured using Pierce™ BCA Assay Kit (ThermoFisher Scientific, USA) using Berthold Mithras^2 LB 943 Multimode Microplate Reader (Berthold Technologies, Germany). Protein concentration calculation (in µg/µL) was done with protein standards supplied by the kit, using the regression line and extrapolating the unknown by GraphPad Prism 9 software. Whole-cell proteins were mixed with 4x Laemmli Buffer with DTT (see Appendix) before loading to gel.

2.5.2 Gel preparation and running

In the preparation of hand-cast gel, 40% Acrylamide/Bis Solution (BIO-RAD Laboratories, USA), TEMED (Sigma-Aldrich, USA), Tris-HCl, SDS, and APS (see Appendix) were used. 10 % separating and 4% stacking gels were prepared according to Table 2.8. Protein samples were loaded to the gel as 20 µg protein per well, and Precision Plus Protein All Blue Pre-Stained Protein Standard (BIO-RAD

Laboratories, USA) was loaded as 2.5 µL per well. Afterward, gel was run at 100V for 2 hours within 1x Running Buffer (see Appendix).

Table 2.8 Components used in preparation of hand-cast gel.

Components	10% Separating Gel	Components	4% Stacking Gel
40% Acrylamide / Bis Solution	1.5 mL	40% Acrylamide / Bis Solution	196 µL
1.5 M Tris-HCl pH 8.8	1.5 mL	0.5 M Tris-HCl pH 8.8	504 µL
10% SDS	60 µL	10% SDS	20 µL
H2O	2.91 mL	H2O	1.27 mL
TEMED	3 µL	TEMED	2 µL
10% APS	30 µL	10% APS	10 µL

2.5.3 Protein transfer

Transfer of the proteins from the gel to PVDF membrane was done by using Hoefer Wet Transfer System (Hoefer Inc, USA). One sponge was placed on the cathode face of transfer module, and a Whatman paper was put on that. Then the gel was placed on Whatman paper followed by carefully positioning of PVDF membrane on top of it. One more Whatman paper was put on membrane, and air bubbles were gently removed by roller. Lastly, three sponges were put on Whatman paper, and the anode face of the transfer module was closed up. All components were soaked in 1x Transfer Buffer (see Appendix) before being aligned in the transfer module. The module was placed within the transfer tank filled with pre-chilled 1x Transfer Buffer. The transfer was done at 400 mA for 1 hour at 4°C.

2.5.4 Antibody probing

Before primary antibody probing, the PVDF membrane was incubated with Blocking Solution (see Appendix) at room temperature for 1 hour on a rocker. After blocking, the membrane was briefly washed with 1x TBST (see Appendix) and incubated at 4°C in primary antibody (GPR56 Antibody (G-6) 200 µg/ml or anti-GFP (B-2) (Santa Cruz BT, USA) in TBST (1:500)), overnight on a rocker. Next day, membrane

was washed with TBST 3 times and incubated for 1 hour in secondary antibody m-IgGκ BP-HRP 200 µg/0.5 m in TBST (1:7500) on a rocker at room temperature. After that, the membrane was incubated with SuperSignal™ West Pico PLUS Chemiluminescent Substrate (ThermoFisher Scientific, USA) in the dark for 5 minutes. Finally, the PVDF membrane was imaged by using BIO-RAD ChemiDoc MP Imaging System (BioRad, USA).

2.6 Bioluminescence Resonance Energy Transfer with GRK and Gβ/ɣ Sensors

Tethered peptide agonist (P7) is a kind gift from Assoc. Prof Dr. Salih Özçubukçu, and BRET sensors (Venus 156-239-Gβ1, Venus 1-155-Gɣ2 and masGRK3ct-NanoLuc) are kind gifts from Prof. Dr. Kirill Martemyanov. HEK293 cells were seeded on 24 well plate (see Table 2.7) and transfected with plasmids (see Table 2.9) by using Invitrogen™ Lipofectamine™ LTX Reagent with PLUS™ Reagent. Next day, cells were detached by using pre-warmed BRET Buffer (see Appendix) and centrifuged at 500 x g for 5 minutes. The supernatant was removed, and the cell pellet was gently resuspended in 100 µL of pre-warmed BRET Buffer. Following that, 25 µL of resuspended cells were seeded on a white 96 well microplate as triplicate. Meanwhile, BRET Buffer containing Furimazine (Promega, USA) was prepared with 1:500 ratio, and 25 µL of it was added to each well. Hence, the final Furimazine and BRET Buffer ratio was 1:1000. Immediately after, the **Basal BRET** value was measured by using Berthold Mithras^2 LB 943 Multimode Microplate Reader. Light emitted from Venus was collected by using 540m40BREThs filter, while light emitted from NLuc was collected by using 460m70nanoBRET filter. Basal BRET value was calculated as the ratio of emission signal of Venus to NLuc. After that, 50 µL of BRET Buffer containing Furimazine with 1:1000 ratio and *Stachel* (P7) peptide with 1 mM concentration was added to each well. Thus, the final concentration of *Stachel* was 500 µM., and the **Experimental BRET** value was measured. The Experimental BRET value was calculated in the same way as the

Basal BRET value. Then, the **Net BRET** value was calculated by subtracting the Basal BRET value from the Experimental BRET value. Statistical analysis and graphical representation of the results were performed by using GraphPad Prism 9 software.

Table 2.9 Ratio and amounts of plasmids used in transfection.

Plasmid	GPCR	Gα12	Venus 156-239-Gβ1	Venus 1-155-Gɣ2	masGRK3ct-NanoLuc
Ratio	1	3	1	1	1
Amount	71 ng	213 ng	71 ng	71 ng	71 ng

2.7 Bioluminescence Resonance Energy Transfer with Beta-Arrestin Sensor

BRET sensors (Rluc8-Arrestin-3-Sp1 and mem-linker-citrine-SH3) are kind gifts from Prof. Dr. Nevin A. Lambert. HEK293 cells were seeded on 24 well plate (see Table 2.7) and transfected with plasmids (see Table 2.10) by using Invitrogen™ Lipofectamine™ LTX Reagent with PLUS™ Reagent. The next day, cells were detached using pre-warmed BRET Buffer and centrifuged at 500 x g for 5 minutes. The supernatant was removed, and the cell pellet was gently resuspended in pre-warmed PBS containing 5mM D-glucose. 25 µL of resuspended cells were seeded on a white 96 well microplate as triplicate. Meanwhile, 10 µM Coelenterazine (Gold Biotechnologies, USA) was prepared in PBS containing 5mM D-glucose, and 25 µL of it was added to each well. Hence, the final concentration of Coelenterazine was 5 µM. Following thtat, the Basal BRET value was measured similar to previous BRET measurement by using Berthold Mithras^2 LB 943 Multimode Microplate Reader. Light emitted from Citrine was collected by using 540m40BREThs filter, while light emitted from RLuc8 was collected by using 4880m20BREThs filter. Basal BRET value was calculated as the ratio of emission signal of Venus to NLuc. *Stachel* (P7) mediated activation and Experimental BRET measurement was done similar to

explained in section 2.7 (Bioluminescence Resonance Energy Transfer with Beta-Arrestin Sensor).

Table 2.10 Ratio and amounts of plasmids used in transfection.

Plasmid	Rluc8-Arrestin-3-Sp1	mem-lnker-citrine-SH3	GPCR	GRK2	pcDNA 3.1+
Ratio	1	20	10	20	20
Amount	5 ng	100 ng	50 ng	100 ng	100 ng

CHAPTER 3

RESULTS

3.1 Laser Scanning Confocal Microscopy

HEK293 cells were co-transfected with ADGRG1-L-EGFP tagged and GAP43-mCherry plasmids. The laser scanning confocal microscope images of the cells are shown in Figure 3.1-7. Compared to ADGRG1-L-EGFP, which was assumed to traffic like wild-type receptor as supported by previous functional assays and immunofluorescence images from the literature (Murat, 2021), membrane localization of the receptors carrying BFPP mutations was observed to be decreased. GAP43-mCherry was used to mark the plasma membrane on the cells. Figure 3.1 shows ADGRG1-L-EGFP carrying R38W mutation, located on the N-terminus of the receptor. Comparing to the wild-type, trafficking and colocalizing of R38W mutant with membrane marker GAP43 was disrupted.

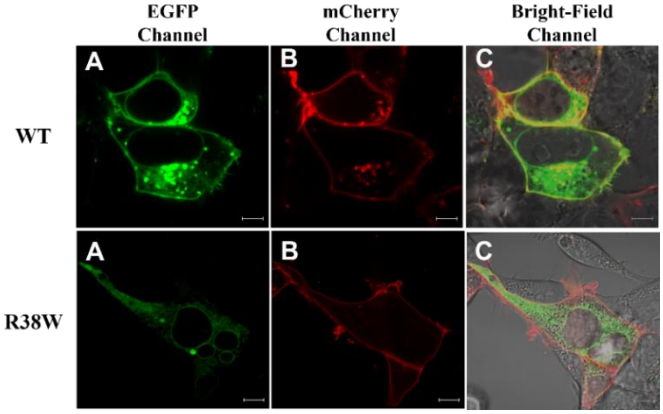

Figure 3.1 Laser Scanning Confocal Microscope images of HEK293 cells transfected with R38W mutant. (A) EGFP tagged ADGRG1/GPR56 receptor; (B) mCherry tagged GAP43 protein; (C) merged bright field image of the cells (C). Scale bar shows 2 μm.

Figure 3.2 shows ADGRG1-L-EGFP carrying Y88C mutation which is also located on the N-terminus of the receptor. Similar to R38W mutant, correct trafficking and colocalizing with membrane marker GAP43 disrupted compared to the wild-type.

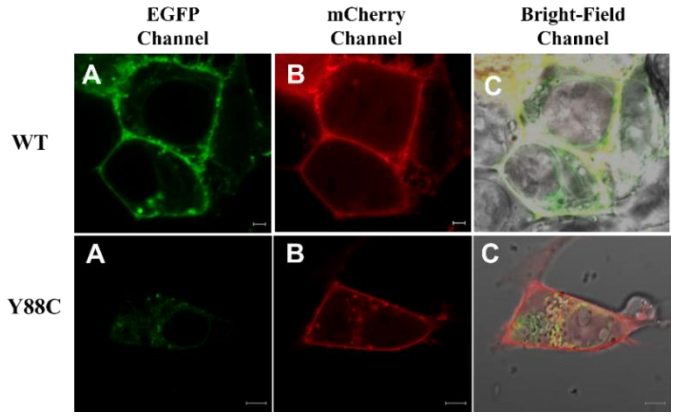

Figure 3.2 Laser Scanning Confocal Microscope images of HEK293 cells transfected with Y88C mutant. (A) EGFP tagged ADGRG1/GPR56 receptor; (B) mCherry tagged GAP43 protein; (C) merged bright field image of the cells (C). Scale bar shows 2 μm.

Figure 3.3 shows ADGRG1-L-EGFP carrying C91S mutation which is the last mutation located on the N-terminus of the receptor. Likewise other mutations located on the N-terminus, this mutation also disrupts the colocalization of the receptor with membrane marker GAP43, compared to the wild-type receptor.

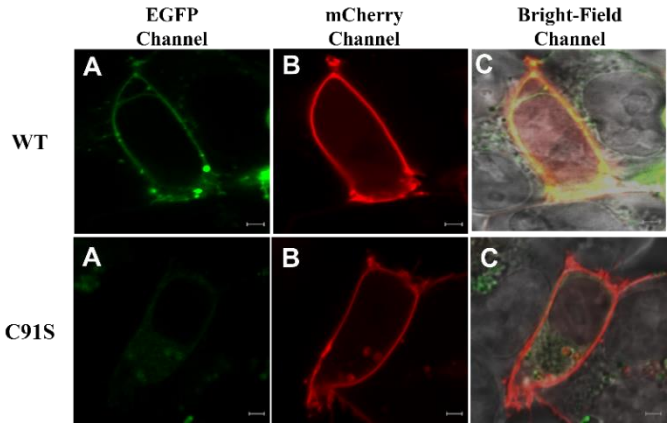

Figure 3.3 Laser Scanning Confocal Microscope images of HEK293 cells transfected with C91S mutant. (A) EGFP tagged ADGRG1/GPR56 receptor; (B) mCherry tagged GAP43 protein; (C) merged bright field image of the cells (C). Scale bar shows 2 μm.

Figure 3.4 shows ADGRG1-L-EGFP carrying C346S mutation, located on the GAIN domain of the receptor. C346S mutation found to disrupts trafficking to the cell membrane and colocalizing with the membrane marker GAP43 when comparing to the wild-type.

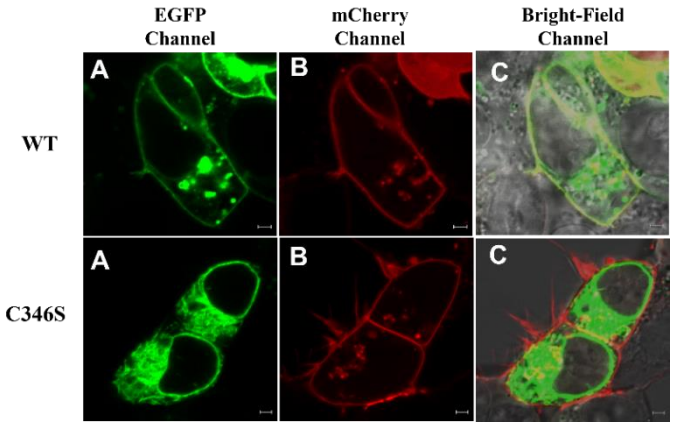

Figure 3.4 Laser Scanning Confocal Microscope images of HEK293 cells transfected with C346S mutant. (A) EGFP tagged ADGRG1/GPR56 receptor; (B) mCherry tagged GAP43 protein; (C) merged bright field image of the cells (C). Scale bar shows 2 μm.

Figure 3.5 shows ADGRG1-L-EGFP carrying W349S mutation located on the GAIN domain. Similar to C346S, W349S mutation disrupts correct trafficking and colocalizing with the membrane marker GAP43 compared to the wild-type.

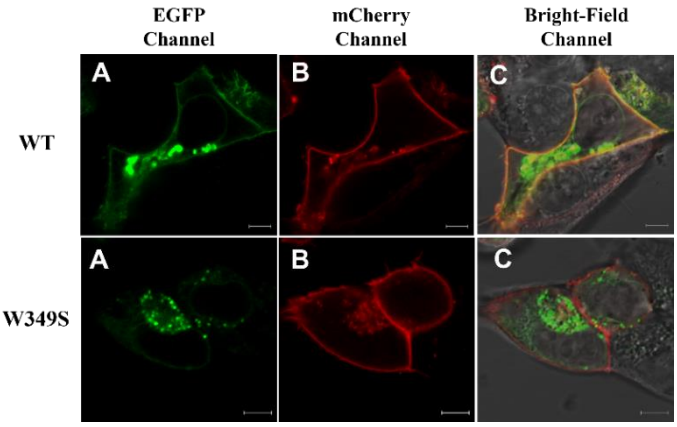

Figure 3.5 Laser Scanning Confocal Microscope images of HEK293 cells transfected with W349S mutant. (A) EGFP tagged ADGRG1/GPR56 receptor; (B) mCherry tagged GAP43 protein; (C) merged bright field image of the cells (C). Scale bar shows 2 μm.

Figure 3.6 shows ADGRG1-L-EGFP carrying R565W mutation, located on the second extracellular loop of the receptor. This mutation also interrupts correct trafficking to the cell membrane and colocalizing with the membrane marker GAP43 comparing with the wild-type.

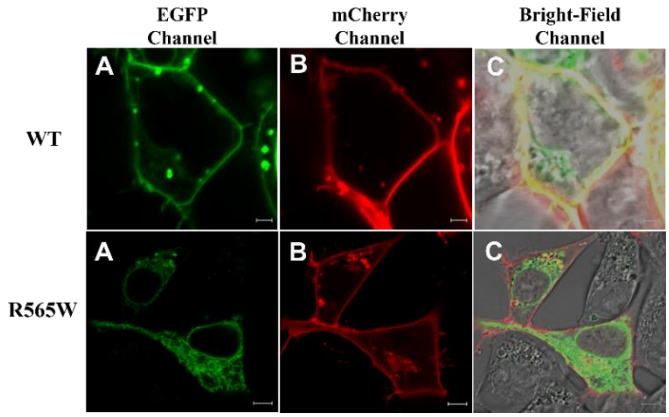

Figure 3.6 Laser Scanning Confocal Microscope images of HEK293 cells transfected with R565W mutant. (A) EGFP tagged ADGRG1/GPR56 receptor; (B) mCherry tagged GAP43 protein; (C) merged bright field image of the cells (C). Scale bar shows 2 μm.

Finally, Figure 3.6 shows ADGRG1-L-EGFP carrying L640R mutation, located on the third extracellular loop of the receptor. Like all other BFPP mutations, L640R interrupts correct trafficking and colocalizing with GAP43 compared to the wild-type receptor.

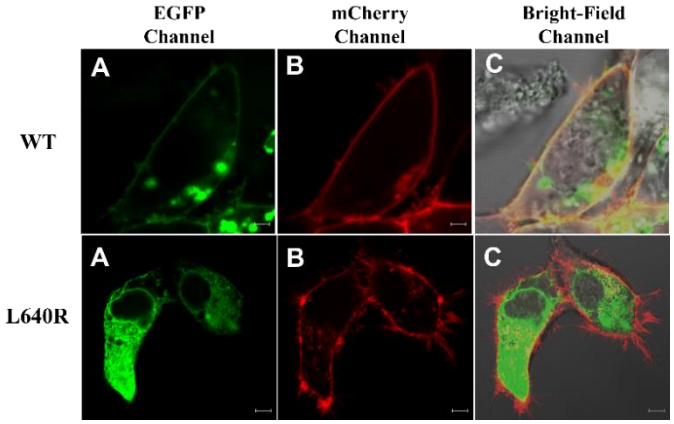

Figure 3.7 Laser Scanning Confocal Microscope images of HEK293 cells transfected with L640R mutant. (A) EGFP tagged ADGRG1/GPR56 receptor; (B) mCherry tagged GAP43 protein; (C) merged bright field image of the cells (C). Scale bar shows 2 μm.

3.2 Western Blot

Untagged ADGRG1/GPR56 receptors carrying BFPP mutations were resolved on PVDF membrane and treated with anti-GPR56 antibody. Except for Y88C and W349S, all protein bands belonging to BFPP mutants were detected on the blot and shown in Figure 3.8. Also, EGFP tagged ADGRG1/GPR56 receptors carrying BFPP mutations were resolved on PVDF membrane and treated with anti-GFP antibody. Except for C91S, all protein bands belonging to EGFP tagged BFPP mutants were detected on the blot and shown in Figure 3.9.

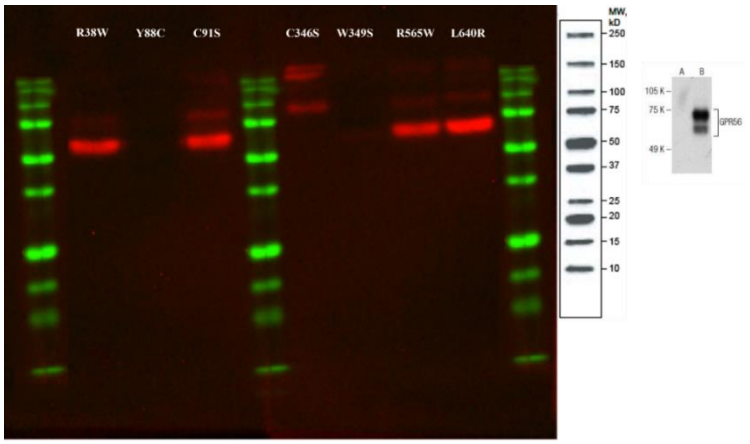

Figure 3.8 Western blot image of ADGRG1/GPR56 protein carrying BFPP mutations. Red bands show protein bands; green bands show protein ladder.

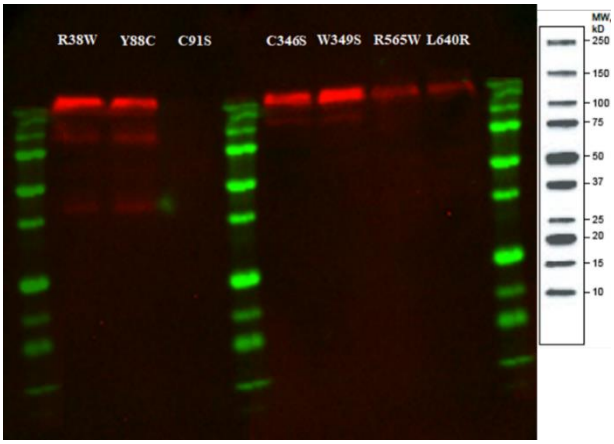

Figure 3.9 Western blot image of EGFP tagged ADGRG1/GPR56 protein carrying BFPP mutations. Red bands show protein bands; green bands show protein ladder.

3.3 BRET

HEK293 cells were transfected with Gβγ and GRK mediated BRET biosensors. The net BRET results of the wild-type and mutant receptors were shown in Figure 3.10.

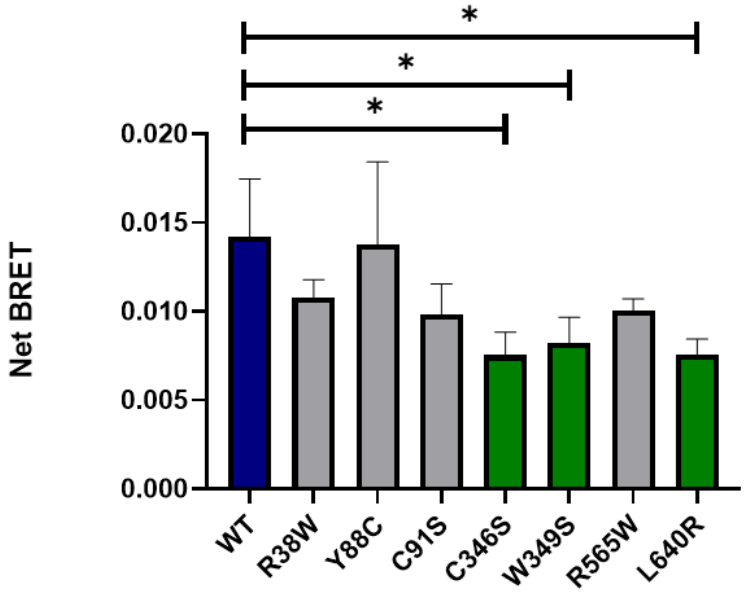

Figure 3.10 Net BRET result of GRK and Gβγ mediated sensors for wild-type and mutant (carrying BFPP mutations) ADGRG1/GPR56 receptor. The standard deviation of the readings was shown by error bars. n=3. $p<0.05$.

The net BRET ratio of wild-type receptors was shown in the blue bar in Figure 3.10. The green bars show the mutants, in which the net BRET ratio was shown to decrease significantly compared with the wild-type. Gray bars in the graph indicate the mutants, in which the net BRET ratio is not changed significantly compared with the wild-type.

HEK293 cells were transfected with beta-arrestin mediated BRET biosensors. The net BRET results of the wild-type and mutant receptors were shown in Figure 3.11.

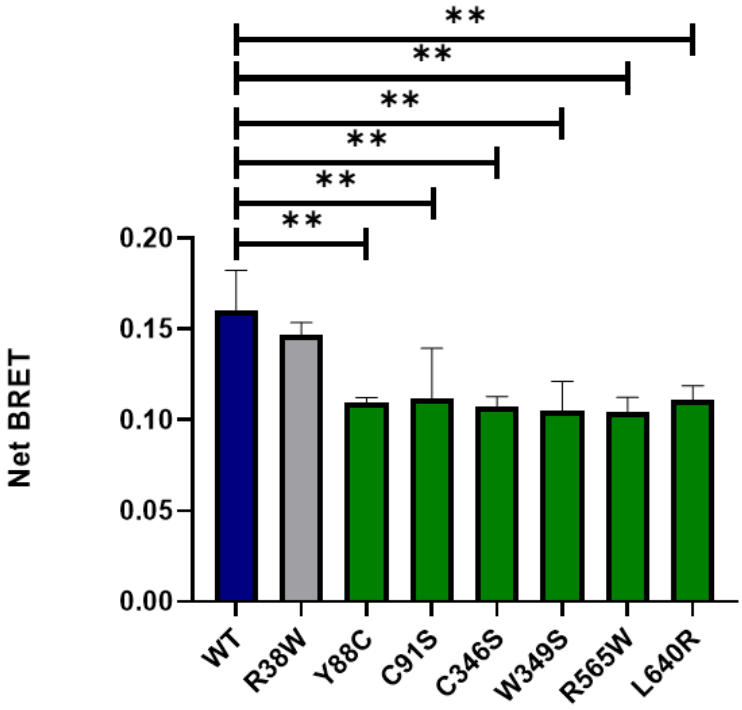

Figure 3.11 Net BRET result of β-arrestin mediated sensors for wild-type and mutant (carrying BFPP mutations) ADGRG1/GPR56 receptor. The standard deviation of the readings was shown by error bars. n=3. $p<0.05$.

The net BRET ratio of wild-type receptors was shown in the blue bar in the figure. The green bars show the mutants, in which the net BRET ratio decreased significantly compared to wild-type. The Gray bar in the graph shows the mutant, in which the net BRET ratio was not changed significantly compared to wild-type.

CHAPTER 4

DISCUSSION

Laser Scanning Confocal Microscope images show double transfected live HEK293 cells with EGFP tagged ADGRG1-L-EGFP receptor and mCherry tagged membrane marker GAP43 protein, GAP43-mCherry. Since both GAP43 and ADGRG1/GPR56 are membrane proteins, it was expected to detect both on the cell membrane. ADGRG1-L-EGFP receptor was detected on the cell membrane, colocalizing with GAP43-mCherry as well as in cytosolic vesicles, presumed to be due to biosynthesis and endocytosis. On the contrary, ADGRG1-L-EGFP constructs carrying BFPP mutations were not detected on the cell membrane compared with the ADGRG1-L-EGFP constructs, presumed to traffic like the wild-type. These observations indicate that BFPP mutations affect the correct localization and trafficking of ADGRG1/GPR56 receptor. In the light of these images, we proposed that receptors carrying BFPP mutations were accumulated in the endoplasmic reticulum–like and vesicular structures. It was clearly seen that the membrane localization was disrupted when compared to the membrane marker GAP43. These results are consistent with the previous literature (Chiang et al., 2011; Jin et al., 2007) using immunofluorescence.

The expression of ADGRG1/GPR56 receptors carrying BFPP mutations was determined using Western Blot Analysis. ADGRG1/GPR56 proteins were detected by using anti GPR56 antibody, that targets an epitope on the N-terminus of the protein. Since ADGRG1/GPR56 was auto-proteolyzed from the GAIN domain (Arac et al., 2012), this antibody only detects the N-terminal part of the receptor. As indicated in Figure 3.8, except Y88C and W349S, protein bands of all mutants were detected on the blot. The possible reason for not detecting the bands of the proteins carrying Y88C and W349S mutations is that; these mutations may decrease the

expression of the receptor or may affect the topology of the binding site of the primary antibody. ADGRG1/GPR56 proteins, tagged with L-EGFP from the C-terminus and carrying the Y88C or W349S mutations, were detected on the blot when treated with GFP antibody (Figure 3.9), which supports the speculation mentioned above. Receptors carrying R38W, C91S, R565W, and L640R mutations were detected between 50-75 kDa, which correspond to the N-terminus of the receptor (~55 kDa). Faded protein bands were also detected between 75-100 kDa, which indicates full length (not cleaved by autoproteolysis) state of the receptor (~77 kDa), and very faded protein bands were detected above 250 kDa, which may indicate the protein aggregates, that could not run through the blot. On the other hand, these bands might be the oligomeric states of the receptors. C346S mutant was only detected between 75-100 kDa and above 250 kDa, and no bands were detected, which correspond to the N-terminus of the receptor. This result is consistent with the literature stating that C346S mutation results in autoproteolysis deficiency (Chiang et al., 2011; Jin et al., 2007).

In order to detect the C-terminal part of the receptor ADGRG1-L-EGFP, these constructs were probed by anti-GFP antibody. As shown in Figure 3.3, protein bands of all mutants, except C91S, were resolved on the blot. The possible reason for not being able to detect C91S mutant is an experimental error since the proteins can be seen in confocal microscope images (Figure 3.3). Protein bands belonging to the C-terminal of the receptor are typically detected around 45, 25, and 15 kDa in size because ADGRG1/GPR56 is subjected to post-translational processing and proteolysis (Paavola, Stephenson, Ritter, Alter, & Hall, 2011). Receptors carrying R38W and Y88C mutations were detected between 37-50 kDa. Considering the calculated molecular weight of the C-terminal domain of the receptor is 15 kDa, and EGFP is ~27 kDa (Arpino, Rizkallah, & Jones, 2012), EGFP tagged C-terminus of the receptor was resolved as faded bands on the blot as expected (~42 kDa in total). Faded bands were also detected between 75-100 kDa, presumed to be the dimers of receptor C-terminal domains. Also, brighter bands above 250 kDa alleged to

correspond the higher oligomeric states of the receptor. Receptors carrying C346S and W349S mutations were detected as faint bands between 100-150 kDa, which might indicate trimeric form of the receptors (~129 kDa). There were also brighter protein bands detected above 250 kDa, which might correspond to higher oligomeric states of the receptors as well as protein aggregates. Normally, protein bands belonging to oligomeric states could not be detected by SDS-PAGE. However, highly hydrophobic proteins such as GPCRs can remain in oligomeric states even under these denaturing conditions (Guo et al., 2017). Lastly, faded protein bands of receptors carrying R565W and L640R mutations were only detected as higher bands above 250 kDa, again presumed to correspond to the receptor oligomers. Overall, it can be speculated that C-terminal domains of the receptors carrying C346S, W349S, R565W, and L640R mutations tend to exist in oligomeric forms; while R38W and Y88C mutants were also resolved as monomers and as receptor oligomers. These results are consistent with the previous literature work (Chiang et al., 2011).

Investigating the activation of ADGRG1/GPR56 receptor-Gα12 coupling was done by using Gβɣ and GRK BRET biosensors (Masuho et al., 2020). *Stachel* (P7) peptide was used as a peptide agonist to induce the activation. Figure 3.10 shows the net BRET ratios of the wild-type and untagged BFPP mutant receptors. Comparing the wild-type receptors C346S, W349S, and L640R mutants showed significantly lower net BRET ratios. It is reported that, ADGRG1/GPR56 couples to Gα12/13 and activates the RhoA pathway upon ligand binding, hence preventing over-migration of neurons and providing proper cerebral cortex lamination (Luo et al., 2011). Additionally, by coupling with Gα12/13 and activating the RhoA pathway, ADGRG1/GPR56 plays a role in the myelination of peripheral nervous system neurons by cytoskeletal remodeling in Schwann cells (Ackerman et al., 2018). Our findings show that, C346S, W349S and L640R mutants failed to couple with Gα12 compared to the wild-type receptor. Thus, it can be speculated that these three mutations individually inhibit proper cerebral cortex lamination and neuronal migration in the brain, as well as myelination of peripheral nervous system neurons

during the development. It was also reported that, BFPP patients carrying C346S mutation show microcephaly (Piao et al., 2005). Our laser scanning confocal microscope results showed that ADGRG1/GPR56 protein carrying C346S mutation was located on endoplasmic reticulum-like vesicular structures. Therefore, it can be speculated that this mutation makes the protein accumulate in endoplasmic reticulum and could result in ER stress. As a result, this mutation may disrupt the normal function of the ER and hence, the homeostasis of the cell. However, it still needs to be verified that this mutant protein is located on ER by examining its colocalization with an ER marker protein. Furthermore, since the C346S, W349S and L640R mutations prevent the receptor couple with Gα12, our work can be a promising starting point for developing a drug molecule which can activate the receptor, hence provides coupling with Gα12.

Beta-arrestin recruitment was assessed by applying beta-arrestin BRET biosensors (Donthamsetti et al., 2015). *Stachel* (P7) peptide was used as a peptide agonist to induce receptor activation, hence beta-arrestin recruitment. Figure 3.11 shows the net BRET ratios of the wild-type and untagged BFPP mutant receptors. Comparing the mutant receptors with the wild-type, except R38W, all mutants showed significantly lower net BRET ratios. This result suggests that these mutations decrease the potential of the receptor to recruit beta-arrestin. Since beta-arrestin recruitment plays role in receptor desensitization by bringing the activated receptor into the clathrin coated-pits and hence supresses the overstimulation of the receptor (T. Wang et al., 2004), it can be speculated that, except R38W mutation, all BFPP mutations disrupt the correct signalling for beta-arrestin recruitment, and hence receptor internalization and re-cycling. Thus, normal regulation of receptor activation fails, and cellular homeostasis is disrupted. As a result, it can be speculated that, the normal function of the receptor is prevented by these mutations during the development. Again, our findings can be a starting point to develop a drug molecule which can rescue the beta-arrestin recruitment of the receptor.

Overall, we examined each mutation in a mechanistic manner by using the mutant constructs *in vitro*. Our work, approaches the effect of these mutations on trafficking, membrane localization and signaling of the receptor. Our confocal microscope images show that, all mutations disrupt the membrane localization of the receptor compared to wild-type. Western blot images also show that, expression of untagged C346S mutant is decreased, and autoproteolysis of the receptor is also disrupted by this mutation. Additionally, BRET biosensors used to investigate coupling the mutant receptors with, Gα12 and betta-arrestin recruitment mediated by receptor activation. Our results propose that, C346S, W349S and L640R mutations significantly decrease the coupling potential of the receptor with Gα12. On the other hand, all mutations cause significant decrease in beta-arrestin recruitment mediated by receptor activation. These findings would lighten the molecular mechanisms and biochemical properties of the disease, as well as the importance of ADGRG1/GPR56 in proper development and functioning of the brain. Moreover, our findings would be a promising starting point for a drug development for BFPP.

CHAPTER 5

CONCLUSION

Bilateral frontoparietal polymicrogyri (BFPP) is a monogenetic autosomal recessive disease that has been associated with ADGRG1/GPR56 receptor. Certain mutations in ADGRG1/GPR56 are detected in BFPP patients (Piao et al., 2002; Piao et al., 2005). Eight missense mutations (R38W, Y88C, C91S, C346S, W349S, R565W, L640R) were examined in this thesis. In order to investigate the effect of BFPP mutations on trafficking ADGRG1/GPR56 receptor; the arofementioned mutations were induced on both wild-type, and EGFP (with linker sequence, L) tagged ADGRG1/GPR56 (ADGRG1-L-EGFP) receptors by using site-directed mutagenesis with two primers. Plasmids carrying mutant ADGRG1-L-EGFP receptor and mCherry tagged membrane marker protein GAP43 (GAP43-mCherry) were used in the transient transfection of HEK293. Laser scanning confocal microscopy results suggested that BFPP mutations affect the correct localization and trafficking of ADGRG1/GPR56 receptor, and it was clearly seen that the membrane localization disrupted when compared to the membrane marker GAP43. We proposed that receptors carrying BFPP mutations were accumulated in the endoplasmic reticulum-like vesicular structures. However, it still needs to be examined by using organelle markers to determine whether our speculation is correct or not. Our future studies aim at investigating the colocalization of mutant ADGRG1/GPR56 receptors with ER and Golgi markers.

Western Blot Analysis was used to assess the expression of ADGRG1/GPR56 receptors with BFPP mutations. Anti-GPR56 antibodies, which target an epitope on the N-terminus of the protein, were used to detect ADGRG1/GPR56 proteins. Because the GAIN domain of ADGRG1/GPR56 was auto-proteolyzed, this antibody only recognizes the N-terminal portion of the receptor (Arac et al., 2012). On the

blot, all mutant proteins were resolved with the exception of Y88C and W349S. In addition to higher oligomeric forms, proteins with the R38W, C91S, R565W, and L640R mutations were shown to be in the right size. The presence of the C346S mutation in the receptor's full-length size is consistent with the literature findings, which claims that it causes autoproteolysis deficiency (Chiang et al., 2011; Jin et al., 2007). The C-terminal portion of the receptor ADGRG1-L-EGFP was detected using an anti-GFP antibody. Except for C91S, all mutant proteins were resolved on the blot. While R38W and Y88C mutants were also resolved as receptor monomers and oligomers, the C-terminal domains of the receptors containing the C346S, W349S, R565W, and L640R mutations appear to have a tendency to exist in oligomeric forms. These results are consistent with the previous literature work (Chiang et al., 2011).

Gβ/ɣ and GRK-BRET biosensors were used to investigate the activation of the ADGRG1/GPR56 receptor-Gα12 coupling (Masuho et al., 2020). These sensors were transfected into HEK 293 cells for this purpose. Following that, the activation was induced using the peptide agonist *Stachel* (P7). As a result, when compared to the wild-type receptors, the mutant C346S, W349S, and L640R receptors had significantly reduced net BRET ratios. According to this finding, these mutations reduce the receptor's ability to couple with Gα12. Thus, the function of the receptor due to coupling with Gα12 and hence RhoA and mTOR pathways is disrupted by these three mutations.

Beta-arrestin recruitment was investigated by using beta-arrestin BRET biosensors (Donthamsetti et al., 2015). For this purpose, HEK 293 cells were transfected with these sensors. Again, *Stachel* (P7) peptide was used as the peptide agonist to induce the receptor activation, hence beta-arrestin recruitment. As a result, all mutant receptors, except the one carrying R38W mutation, displayed significantly reduced net BRET ratios when compared to the wild-type. This finding implies that these

mutations reduce the receptor's capacity to recruit beta-arrestin. Since beta-arrestin recruitment is prevented by the mutations, desensitization of the receptor is inhibited, and normal function and signaling of the receptor is disrupted.

Future Studies

We have shown that, BFPP mutations decreases the cell surface expression of ADGRG1/GPR56 protein, by comparing its colocalization with membrane marker GAP43. We are also planning to investigate its colocalization with endoplasmic reticulum and Golgi markers. There are different methods, which provide to investigate the cell surface expression of a protein. One of these methods are cell surface Enzyme-linked Immunosorbent Assay (ELISA) (Bishop & Hwang, 1992). Alternatively, immunofluorescence flow cytometry is another tool provides investigating the cell surface expression of a protein (Posey, 1990). We are planning to integrate these methods to our research. We are also searching for an antibody, which detects the C-terminal region of ADGRG1/GPR56.

REFERENCES

Ackerman, S. D., Garcia, C., Piao, X., Gutmann, D. H., & Monk, K. R. (2015). The adhesion GPCR Gpr56 regulates oligodendrocyte development via interactions with Galpha12/13 and RhoA. *Nat Commun, 6*, 6122. doi:10.1038/ncomms7122

Ackerman, S. D., Luo, R., Poitelon, Y., Mogha, A., Harty, B. L., D'Rozario, M., . . . Monk, K. R. (2018). GPR56/ADGRG1 regulates development and maintenance of peripheral myelin. *J Exp Med, 215*(3), 941-961. doi:10.1084/jem.20161714

Arac, D., Boucard, A. A., Bolliger, M. F., Nguyen, J., Soltis, S. M., Sudhof, T. C., & Brunger, A. T. (2012). A novel evolutionarily conserved domain of cell-adhesion GPCRs mediates autoproteolysis. *EMBO J, 31*(6), 1364-1378. doi:10.1038/emboj.2012.26

Arcos-Burgos, M., & Muenke, M. (2010). Toward a better understanding of ADHD: LPHN3 gene variants and the susceptibility to develop ADHD. *Atten Defic Hyperact Disord, 2*(3), 139-147. doi:10.1007/s12402-010-0030-2

Arpino, J. A., Rizkallah, P. J., & Jones, D. D. (2012). Crystal structure of enhanced green fluorescent protein to 1.35 A resolution reveals alternative conformations for Glu222. *PLoS One, 7*(10), e47132. doi:10.1371/journal.pone.0047132

Bayin, N. S., Frenster, J. D., Kane, J. R., Rubenstein, J., Modrek, A. S., Baitalmal, R., . . . Placantonakis, D. G. (2016). GPR133 (ADGRD1), an adhesion G-protein-coupled receptor, is necessary for glioblastoma growth. *Oncogenesis, 5*(10), e263. doi:10.1038/oncsis.2016.63

Becker, S., Wandel, E., Wobus, M., Schneider, R., Amasheh, S., Sittig, D., . . . Aust, G. (2010). Overexpression of CD97 in intestinal epithelial cells of transgenic mice attenuates colitis by strengthening adherens junctions. *PLoS One, 5*(1), e8507. doi:10.1371/journal.pone.0008507

Bennett, M. L., Bennett, F. C., Liddelow, S. A., Ajami, B., Zamanian, J. L., Fernhoff, N. B., . . . Barres, B. A. (2016). New tools for studying microglia in the mouse and human CNS. *Proc Natl Acad Sci U S A, 113*(12), E1738-1746. doi:10.1073/pnas.1525528113

Bishop, G. A., & Hwang, J. (1992). Use of a cellular ELISA for the detection of cell surface antigens. *Biotechniques, 12*(3), 326-330. Retrieved from https://www.ncbi.nlm.nih.gov/pubmed/1571137

Bjarnadottir, T. K., Geirardsdottir, K., Ingemansson, M., Mirza, M. A., Fredriksson, R., & Schioth, H. B. (2007). Identification of novel splice variants of Adhesion G protein-coupled receptors. *Gene, 387*(1-2), 38-48. doi:10.1016/j.gene.2006.07.039

Boyden, S. E., Desai, A., Cruse, G., Young, M. L., Bolan, H. C., Scott, L. M., . . . Komarow, H. D. (2016). Vibratory Urticaria Associated with a Missense Variant in ADGRE2. *N Engl J Med, 374*(7), 656-663. doi:10.1056/NEJMoa1500611

Boyden, S. E., Metcalfe, D. D., & Komarow, H. D. (2016). Vibratory Urticaria and ADGRE2. *N Engl J Med, 375*(1), 95. doi:10.1056/NEJMc1604757

Bridges, J. P., Ludwig, M. G., Mueller, M., Kinzel, B., Sato, A., Xu, Y., . . . Ikegami, M. (2013). Orphan G protein-coupled receptor GPR116 regulates pulmonary surfactant pool size. *Am J Respir Cell Mol Biol, 49*(3), 348-357. doi:10.1165/rcmb.2012-0439OC

Chiang, N. Y., Hsiao, C. C., Huang, Y. S., Chen, H. Y., Hsieh, I. J., Chang, G. W., & Lin, H. H. (2011). Disease-associated GPR56 mutations cause bilateral frontoparietal polymicrogyria via multiple mechanisms. *J Biol Chem, 286*(16), 14215-14225. doi:10.1074/jbc.M110.183830

Demberg, L. M., Winkler, J., Wilde, C., Simon, K. U., Schon, J., Rothemund, S., . . . Liebscher, I. (2017). Activation of Adhesion G Protein-coupled Receptors: AGONIST SPECIFICITY OF STACHEL SEQUENCE-DERIVED PEPTIDES. *J Biol Chem, 292*(11), 4383-4394. doi:10.1074/jbc.M116.763656

Donthamsetti, P., Quejada, J. R., Javitch, J. A., Gurevich, V. V., & Lambert, N. A. (2015). Using Bioluminescence Resonance Energy Transfer (BRET) to Characterize Agonist-Induced Arrestin Recruitment to Modified and Unmodified G Protein-Coupled Receptors. *Curr Protoc Pharmacol, 70*, 2 14 11-12 14 14. doi:10.1002/0471141755.ph0214s70

Duc, N. M., Kim, H. R., & Chung, K. Y. (2015). Structural mechanism of G protein activation by G protein-coupled receptor. *Eur J Pharmacol, 763*(Pt B), 214-222. doi:10.1016/j.ejphar.2015.05.016

Favara, D. M., Banham, A. H., & Harris, A. L. (2014). A review of ELTD1, a pro-angiogenic adhesion GPCR. *Biochem Soc Trans, 42*(6), 1658-1664. doi:10.1042/BST20140216

Fredriksson, R., Gloriam, D. E., Hoglund, P. J., Lagerstrom, M. C., & Schioth, H. B. (2003). There exist at least 30 human G-protein-coupled receptors with long Ser/Thr-rich N-termini. *Biochem Biophys Res Commun, 301*(3), 725-734. doi:10.1016/s0006-291x(03)00026-3

Fredriksson, R., Lagerstrom, M. C., Lundin, L. G., & Schioth, H. B. (2003). The G-protein-coupled receptors in the human genome form five main families. Phylogenetic analysis, paralogon groups, and fingerprints. *Mol Pharmacol, 63*(6), 1256-1272. doi:10.1124/mol.63.6.1256

Gad, A. A., & Balenga, N. (2020). The Emerging Role of Adhesion GPCRs in Cancer. *ACS Pharmacol Transl Sci, 3*(1), 29-42. doi:10.1021/acsptsci.9b00093

Gales, C., Van Durm, J. J., Schaak, S., Pontier, S., Percherancier, Y., Audet, M., . . . Bouvier, M. (2006). Probing the activation-promoted structural rearrangements in preassembled receptor-G protein complexes. *Nat Struct Mol Biol, 13*(9), 778-786. doi:10.1038/nsmb1134

Giera, S., Deng, Y., Luo, R., Ackerman, S. D., Mogha, A., Monk, K. R., . . . Piao, X. (2015). The adhesion G protein-coupled receptor GPR56 is a cell-autonomous regulator of oligodendrocyte development. *Nat Commun, 6*, 6121. doi:10.1038/ncomms7121

Giera, S., Luo, R., Ying, Y., Ackerman, S. D., Jeong, S. J., Stoveken, H. M., . . . Piao, X. (2018). Microglial transglutaminase-2 drives myelination and myelin repair via GPR56/ADGRG1 in oligodendrocyte precursor cells. *Elife, 7*. doi:10.7554/eLife.33385

GPCRdb. (2022, June 23). GPCRdb. Retrieved from https://gpcrdb.org/drugs/drugstatistics

Guo, H., An, S., Ward, R., Yang, Y., Liu, Y., Guo, X. X., . . . Xu, T. R. (2017). Methods used to study the oligomeric structure of G-protein-coupled receptors. *Biosci Rep, 37*(2). doi:10.1042/BSR20160547

Hamann, J., Eichler, W., Hamann, D., Kerstens, H. M., Poddighe, P. J., Hoovers, J. M., . . . van Lier, R. A. (1995). Expression cloning and chromosomal mapping of the leukocyte activation antigen CD97, a new seven-span transmembrane molecule of the secretion receptor superfamily with an unusual extracellular domain. *J Immunol, 155*(4), 1942-1950. Retrieved from https://www.ncbi.nlm.nih.gov/pubmed/7636245

Hauser, A. S., Chavali, S., Masuho, I., Jahn, L. J., Martemyanov, K. A., Gloriam, D. E., & Babu, M. M. (2018). Pharmacogenomics of GPCR Drug Targets. *Cell, 172*(1-2), 41-54 e19. doi:10.1016/j.cell.2017.11.033

Hill, S. J. (2006). G-protein-coupled receptors: past, present and future. *Br J Pharmacol, 147 Suppl 1*, S27-37. doi:10.1038/sj.bjp.0706455

Hsiao, C. C., Chu, T. Y., Wu, C. J., van den Biggelaar, M., Pabst, C., Hebert, J., . . . Lin, H. H. (2018). The Adhesion G Protein-Coupled Receptor GPR97/ADGRG3 Is Expressed in Human Granulocytes and Triggers Antimicrobial Effector Functions. *Front Immunol, 9*, 2830. doi:10.3389/fimmu.2018.02830

Iguchi, T., Sakata, K., Yoshizaki, K., Tago, K., Mizuno, N., & Itoh, H. (2008). Orphan G protein-coupled receptor GPR56 regulates neural progenitor cell migration via a G alpha 12/13 and Rho pathway. *J Biol Chem, 283*(21), 14469-14478. doi:10.1074/jbc.M708919200

Jeong, S. J., Luo, R., Li, S., Strokes, N., & Piao, X. (2012). Characterization of G protein-coupled receptor 56 protein expression in the mouse developing neocortex. *J Comp Neurol, 520*(13), 2930-2940. doi:10.1002/cne.23076

Jeong, S. J., Luo, R., Singer, K., Giera, S., Kreidberg, J., Kiyozumi, D., . . . Piao, X. (2013). GPR56 functions together with alpha3beta1 integrin in regulating cerebral cortical development. *PLoS One, 8*(7), e68781. doi:10.1371/journal.pone.0068781

Jin, Z., Tietjen, I., Bu, L., Liu-Yesucevitz, L., Gaur, S. K., Walsh, C. A., & Piao, X. (2007). Disease-associated mutations affect GPR56 protein trafficking and cell surface expression. *Hum Mol Genet, 16*(16), 1972-1985. doi:10.1093/hmg/ddm144

Kaur, B., Brat, D. J., Devi, N. S., & Van Meir, E. G. (2005). Vasculostatin, a proteolytic fragment of brain angiogenesis inhibitor 1, is an antiangiogenic and antitumorigenic factor. *Oncogene, 24*(22), 3632-3642. doi:10.1038/sj.onc.1208317

Kishore, A., & Hall, R. A. (2017). Disease-associated extracellular loop mutations in the adhesion G protein-coupled receptor G1 (ADGRG1; GPR56) differentially regulate downstream signaling. *J Biol Chem, 292*(23), 9711-9720. doi:10.1074/jbc.M117.780551

Kishore, A., Purcell, R. H., Nassiri-Toosi, Z., & Hall, R. A. (2016). Stalk-dependent and Stalk-independent Signaling by the Adhesion G Protein-coupled Receptors GPR56 (ADGRG1) and BAI1 (ADGRB1). *J Biol Chem, 291*(7), 3385-3394. doi:10.1074/jbc.M115.689349

Knierim, A. B., Rothe, J., Cakir, M. V., Lede, V., Wilde, C., Liebscher, I., . . . Schoneberg, T. (2019). Genetic basis of functional variability in adhesion G protein-coupled receptors. *Sci Rep, 9*(1), 11036. doi:10.1038/s41598-019-46265-x

Kobayashi, H., & Bouvier, M. (2021). Bioluminescence Resonance Energy Transfer (BRET) Imaging in Living Cells: Image Acquisition and Quantification. *Methods Mol Biol, 2274*, 305-314. doi:10.1007/978-1-0716-1258-3_26

Kobilka, B. K. (2007). G protein coupled receptor structure and activation. *Biochim Biophys Acta, 1768*(4), 794-807. doi:10.1016/j.bbamem.2006.10.021

Kuhn, H. (1978). Light-regulated binding of rhodopsin kinase and other proteins to cattle photoreceptor membranes. *Biochemistry, 17*(21), 4389-4395. doi:10.1021/bi00614a006

Kuhn, H., Hall, S. W., & Wilden, U. (1984). Light-induced binding of 48-kDa protein to photoreceptor membranes is highly enhanced by phosphorylation of rhodopsin. *FEBS Lett, 176*(2), 473-478. doi:10.1016/0014-5793(84)81221-1

Langenhan, T., Aust, G., & Hamann, J. (2013). Sticky signaling--adhesion class G protein-coupled receptors take the stage. *Sci Signal, 6*(276), re3. doi:10.1126/scisignal.2003825

Langenhan, T., Piao, X., & Monk, K. R. (2016). Adhesion G protein-coupled receptors in nervous system development and disease. *Nat Rev Neurosci, 17*(9), 550-561. doi:10.1038/nrn.2016.86

Lee, J. W., Huang, B. X., Kwon, H., Rashid, M. A., Kharebava, G., Desai, A., . . . Kim, H. Y. (2016). Orphan GPR110 (ADGRF1) targeted by N-docosahexaenoylethanolamine in development of neurons and cognitive function. *Nat Commun, 7*, 13123. doi:10.1038/ncomms13123

Lefkowitz, R. J. (2000). The superfamily of heptahelical receptors. *Nat Cell Biol, 2*(7), E133-136. doi:10.1038/35017152

Li, T., Chiou, B., Gilman, C. K., Luo, R., Koshi, T., Yu, D., . . . Piao, X. (2020). A splicing isoform of GPR56 mediates microglial synaptic refinement via phosphatidylserine binding. *EMBO J, 39*(16), e104136. doi:10.15252/embj.2019104136

Liebscher, I., Cevheroglu, O., Hsiao, C. C., Maia, A. F., Schihada, H., Scholz, N., . . . Promel, S. (2021). A guide to adhesion GPCR research. *FEBS J*. doi:10.1111/febs.16258

Lindenmaier, L. B., Parmentier, N., Guo, C., Tissir, F., & Wright, K. M. (2019). Dystroglycan is a scaffold for extracellular axon guidance decisions. *Elife, 8*. doi:10.7554/eLife.42143

Little, K. D., Hemler, M. E., & Stipp, C. S. (2004). Dynamic regulation of a GPCR-tetraspanin-G protein complex on intact cells: central role of CD81 in facilitating GPR56-Galpha q/11 association. *Mol Biol Cell, 15*(5), 2375-2387. doi:10.1091/mbc.e03-12-0886

Liu, M., Parker, R. M., Darby, K., Eyre, H. J., Copeland, N. G., Crawford, J., . . . Herzog, H. (1999). GPR56, a novel secretin-like human G-protein-coupled receptor gene. *Genomics, 55*(3), 296-305. doi:10.1006/geno.1998.5644

Luo, R., Jeong, S. J., Jin, Z., Strokes, N., Li, S., & Piao, X. (2011). G protein-coupled receptor 56 and collagen III, a receptor-ligand pair, regulates cortical development and lamination. *Proc Natl Acad Sci U S A, 108*(31), 12925-12930. doi:10.1073/pnas.1104821108

Masuho, I., Skamangas, N. K., & Martemyanov, K. A. (2020). Live cell optical assay for precise characterization of receptors coupling to Galpha12. *Basic Clin Pharmacol Toxicol, 126 Suppl 6*, 88-95. doi:10.1111/bcpt.13228

Meza-Aguilar, D. G., & Boucard, A. A. (2014). Latrophilins updated. *Biomol Concepts, 5*(6), 457-478. doi:10.1515/bmc-2014-0032

Milligan, G. (2003). Constitutive activity and inverse agonists of G protein-coupled receptors: a current perspective. *Mol Pharmacol, 64*(6), 1271-1276. doi:10.1124/mol.64.6.1271

Mogha, A., Harty, B. L., Carlin, D., Joseph, J., Sanchez, N. E., Suter, U., . . . Monk, K. R. (2016). Gpr126/Adgrg6 Has Schwann Cell Autonomous and Nonautonomous Functions in Peripheral Nerve Injury and Repair. *J Neurosci, 36*(49), 12351-12367. doi:10.1523/JNEUROSCI.3854-15.2016

Monk, K. R., Oshima, K., Jors, S., Heller, S., & Talbot, W. S. (2011). Gpr126 is essential for peripheral nerve development and myelination in mammals. *Development*, *138*(13), 2673-2680. doi:10.1242/dev.062224

Murat, M. (2021). *A Brighter Method to Illuminate the Dark Side of Adhesion G Protein-Coupled Receptors: Detection of the ADGRG1 Dimers by Bioluminescence Resonance Energy Transfer (BRET).* (Master's dissertation). Middle East Technical University, Turkey. Retrieved from https://open.metu.edu.tr/handle/11511/92438

Paavola, K. J., Stephenson, J. R., Ritter, S. L., Alter, S. P., & Hall, R. A. (2011). The N terminus of the adhesion G protein-coupled receptor GPR56 controls receptor signaling activity. *J Biol Chem*, *286*(33), 28914-28921. doi:10.1074/jbc.M111.247973

Pfister, C., Chabre, M., Plouet, J., Tuyen, V. V., De Kozak, Y., Faure, J. P., & Kuhn, H. (1985). Retinal S antigen identified as the 48K protein regulating light-dependent phosphodiesterase in rods. *Science*, *228*(4701), 891-893. doi:10.1126/science.2988124

Piao, X., Basel-Vanagaite, L., Straussberg, R., Grant, P. E., Pugh, E. W., Doheny, K., . . . Walsh, C. A. (2002). An autosomal recessive form of bilateral frontoparietal polymicrogyria maps to chromosome 16q12.2-21. *Am J Hum Genet*, *70*(4), 1028-1033. doi:10.1086/339552

Piao, X., Chang, B. S., Bodell, A., Woods, K., Benzeev, B., Topcu, M., . . . Walsh, C. A. (2005). Genotype-phenotype analysis of human frontoparietal polymicrogyria syndromes. *Ann Neurol*, *58*(5), 680-687. doi:10.1002/ana.20616

Pierce, K. L., Premont, R. T., & Lefkowitz, R. J. (2002). Seven-transmembrane receptors. *Nat Rev Mol Cell Biol*, *3*(9), 639-650. doi:10.1038/nrm908

Posey, D. H., Jr. (1990). Flow cytometry: past, present, and future. *J Natl Med Assoc*, *82*(8), 581-582. Retrieved from https://www.ncbi.nlm.nih.gov/pubmed/2395178

Salahpour, A., Espinoza, S., Masri, B., Lam, V., Barak, L. S., & Gainetdinov, R. R. (2012). BRET biosensors to study GPCR biology, pharmacology, and signal transduction. *Front Endocrinol (Lausanne)*, *3*, 105. doi:10.3389/fendo.2012.00105

Salzman, G. S., Ackerman, S. D., Ding, C., Koide, A., Leon, K., Luo, R., . . . Arac, D. (2016). Structural Basis for Regulation of GPR56/ADGRG1 by Its Alternatively Spliced Extracellular Domains. *Neuron, 91*(6), 1292-1304. doi:10.1016/j.neuron.2016.08.022

Salzman, G. S., Zhang, S., Gupta, A., Koide, A., Koide, S., & Arac, D. (2017). Stachel-independent modulation of GPR56/ADGRG1 signaling by synthetic ligands directed to its extracellular region. *Proc Natl Acad Sci U S A, 114*(38), 10095-10100. doi:10.1073/pnas.1708810114

Sanders, R. D., Brian, D., & Maze, M. (2008). G-protein-coupled receptors. *Handb Exp Pharmacol*(182), 93-117. doi:10.1007/978-3-540-74806-9_5

Schihada, H., Shekhani, R., & Schulte, G. (2021). Quantitative assessment of constitutive G protein-coupled receptor activity with BRET-based G protein biosensors. *Sci Signal, 14*(699), eabf1653. doi:10.1126/scisignal.abf1653

Schioth, H. B., Nordstrom, K. J., & Fredriksson, R. (2010). The adhesion GPCRs; gene repertoire, phylogeny and evolution. *Adv Exp Med Biol, 706*, 1-13. doi:10.1007/978-1-4419-7913-1_1

Singer, K., Luo, R., Jeong, S. J., & Piao, X. (2013). GPR56 and the developing cerebral cortex: cells, matrix, and neuronal migration. *Mol Neurobiol, 47*(1), 186-196. doi:10.1007/s12035-012-8343-0

Singh, A. K., & Lin, H. H. (2021). The role of GPR56/ADGRG1 in health and disease. *Biomed J, 44*(5), 534-547. doi:10.1016/j.bj.2021.04.012

Stenkamp, R. E., Teller, D. C., & Palczewski, K. (2002). Crystal structure of rhodopsin: a G-protein-coupled receptor. *Chembiochem, 3*(10), 963-967. doi:10.1002/1439-7633(20021004)3:10<963::AID-CBIC963>3.0.CO;2-9

Stoveken, H. M., Hajduczok, A. G., Xu, L., & Tall, G. G. (2015). Adhesion G protein-coupled receptors are activated by exposure of a cryptic tethered agonist. *Proc Natl Acad Sci U S A, 112*(19), 6194-6199. doi:10.1073/pnas.1421785112

Vizurraga, A., Adhikari, R., Yeung, J., Yu, M., & Tall, G. G. (2020). Mechanisms of adhesion G protein-coupled receptor activation. *J Biol Chem, 295*(41), 14065-14083. doi:10.1074/jbc.REV120.007423

Waddell, L. A., Lefevre, L., Bush, S. J., Raper, A., Young, R., Lisowski, Z. M., . . . Hume, D. A. (2018). ADGRE1 (EMR1, F4/80) Is a Rapidly-Evolving Gene Expressed in Mammalian Monocyte-Macrophages. *Front Immunol, 9*, 2246. doi:10.3389/fimmu.2018.02246

Wang, L., Xiao, Y., Tian, T., Jin, L., Lei, Y., Finnell, R. H., & Ren, A. (2018). Digenic variants of planar cell polarity genes in human neural tube defect patients. *Mol Genet Metab, 124*(1), 94-100. doi:10.1016/j.ymgme.2018.03.005

Wang, T., Li, Z., Cvijic, M. E., Krause, C., Zhang, L., & Sum, C. S. (2004). Measurement of beta-Arrestin Recruitment for GPCR Targets. In S. Markossian, A. Grossman, K. Brimacombe, M. Arkin, D. Auld, C. Austin, J. Baell, T. D. Y. Chung, N. P. Coussens, J. L. Dahlin, V. Devanarayan, T. L. Foley, M. Glicksman, J. V. Haas, M. D. Hall, S. Hoare, J. Inglese, P. W. Iversen, S. C. Kales, M. Lal-Nag, Z. Li, J. McGee, O. McManus, T. Riss, P. Saradjian, G. S. Sittampalam, M. Tarselli, O. J. Trask, Jr., Y. Wang, J. R. Weidner, M. J. Wildey, K. Wilson, M. Xia, & X. Xu (Eds.), *Assay Guidance Manual*. Bethesda (MD).

Wang, Y., Fan, X., Zhang, W., Zhang, C., Wang, J., Jiang, T., & Wang, L. (2015). Deficiency of very large G-protein-coupled receptor-1 is a risk factor of tumor-related epilepsy: a whole transcriptome sequencing analysis. *J Neurooncol, 121*(3), 609-616. doi:10.1007/s11060-014-1674-0

Weston, M. D., Luijendijk, M. W., Humphrey, K. D., Moller, C., & Kimberling, W. J. (2004). Mutations in the VLGR1 gene implicate G-protein signaling in the pathogenesis of Usher syndrome type II. *Am J Hum Genet, 74*(2), 357-366. doi:10.1086/381685

White, J. P., Wrann, C. D., Rao, R. R., Nair, S. K., Jedrychowski, M. P., You, J. S., . . . Spiegelman, B. M. (2014). G protein-coupled receptor 56 regulates mechanical overload-induced muscle hypertrophy. *Proc Natl Acad Sci U S A, 111*(44), 15756-15761. doi:10.1073/pnas.1417898111

Wu, P., & Brand, L. (1994). Resonance energy transfer: methods and applications. *Anal Biochem, 218*(1), 1-13. doi:10.1006/abio.1994.1134

Xu, L., Begum, S., Hearn, J. D., & Hynes, R. O. (2006). GPR56, an atypical G protein-coupled receptor, binds tissue transglutaminase, TG2, and inhibits melanoma tumor growth and metastasis. *Proc Natl Acad Sci U S A, 103*(24), 9023-9028. doi:10.1073/pnas.0602681103

Yano, H., Provasi, D., Cai, N. S., Filizola, M., Ferre, S., & Javitch, J. A. (2017). Development of novel biosensors to study receptor-mediated activation of the G-protein alpha subunits Gs and Golf. *J Biol Chem, 292*(49), 19989-19998. doi:10.1074/jbc.M117.800698

Yona, S., Lin, H. H., Dri, P., Davies, J. Q., Hayhoe, R. P., Lewis, S. M., . . . Stacey, M. (2008). Ligation of the adhesion-GPCR EMR2 regulates human neutrophil function. *FASEB J, 22*(3), 741-751. doi:10.1096/fj.07-9435com

Zhang, Y., Chen, K., Sloan, S. A., Bennett, M. L., Scholze, A. R., O'Keeffe, S., . . . Wu, J. Q. (2014). An RNA-sequencing transcriptome and splicing database of glia, neurons, and vascular cells of the cerebral cortex. *J Neurosci, 34*(36), 11929-11947. doi:10.1523/JNEUROSCI.1860-14.2014

Zhu, B., Luo, R., Jin, P., Li, T., Oak, H. C., Giera, S., . . . Piao, X. (2019). GAIN domain-mediated cleavage is required for activation of G protein-coupled receptor 56 (GPR56) by its natural ligands and a small-molecule agonist. *J Biol Chem, 294*(50), 19246-19254. doi:10.1074/jbc.RA119.008234

APPENDICES

A. Plasmid Maps

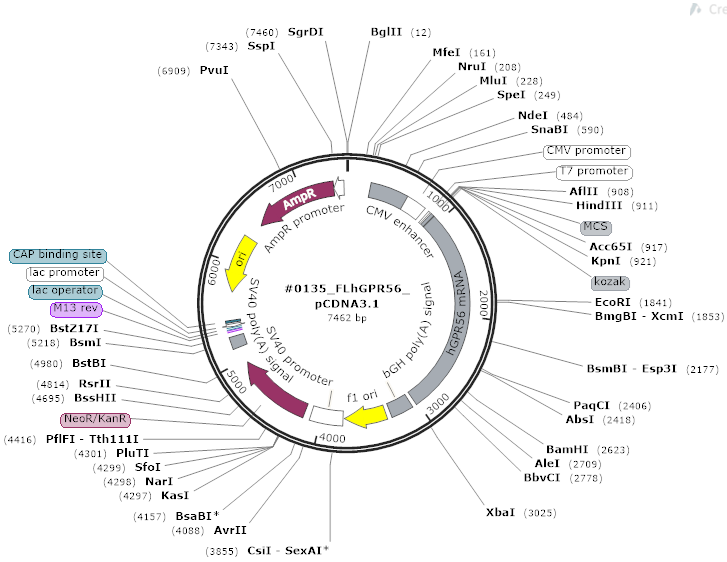

Figure A.1 pcDNA 3.1 + containing human ADGRG1/GPR56.

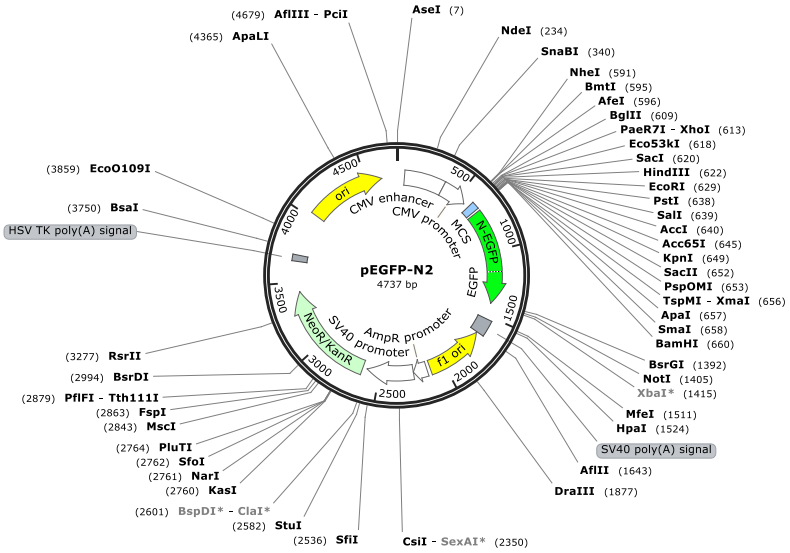

Figure A.2 pcDNA 3.1 + containing EGFP.

B. Sanger Sequencing

Score	Expect	Identities	Gaps	Strand
366 bits(198)	2e-105	200/201(99%)	0/201(0%)	Plus/Plus

```
Query  1    ATGACTCCCCAGTCGCTGCTGCAGACGACACTGTTCCTGCTGAGTCTGCTCTTCCTGGTC  60
            ||||||||||||||||||||||||||||||||||||||||||||||||||||||||||||
Sbjct  110  ATGACTCCCCAGTCGCTGCTGCAGACGACACTGTTCCTGCTGAGTCTGCTCTTCCTGGTC  169

Query  61   CAAGGTGCCCACGGCAGGGGCCACAGGGAAGACTTTCGCTTCTGCAGCCAGCGGAACCAG  120
            ||||||||||||||||||||||||||||||||||||||||||||||||||||||||||||
Sbjct  170  CAAGGTGCCCACGGCAGGGGCCACAGGGAAGACTTTCGCTTCTGCAGCCAGTGGAACCAG  229

Query  121  ACACACAGGAGCAGCCTCCACTACAAACCCACACCAGACCTGCGCATCTCCATCGAGAAC  180
            ||||||||||||||||||||||||||||||||||||||||||||||||||||||||||||
Sbjct  230  ACACACAGGAGCAGCCTCCACTACAAACCCACACCAGACCTGCGCATCTCCATCGAGAAC  289

Query  181  TCCGAAGAGGCCCTCACAGTC  201
            |||||||||||||||||||||
Sbjct  290  TCCGAAGAGGCCCTCACAGTC  310
```

Figure B.1 Sequencing result of R38W mutation on ADGRG1/GPR56. The box shows nucleotide change (112 C > T) on cDNA of the receptor.

Score	Expect	Identities	Gaps	Strand
353 bits(191)	1e-101	193/194(99%)	0/194(0%)	Plus/Plus

```
Query  190  GCCCTCACAGTCCATGCCCCTTTCCCTGCAGCCCACCCTGCTTCCCGATCCTTCCCTGAC  249
            ||||||||||||||||||||||||||||||||||||||||||||||||||||||||||||
Sbjct  1    GCCCTCACAGTCCATGCCCCTTTCCCTGCAGCCCACCCTGCTTCCCGATCCTTCCCTGAC  60

Query  250  CCCAGGGGCCTCTACCACTTCTGCCTCTACTGGAACCGACATGCTGGGAGATTACATCTT  309
            ||||||||||||| ||||||||||||||||||||||||||||||||||||||||||||||
Sbjct  61   CCCAGGGGCCTCTGCCACTTCTGCCTCTACTGGAACCGACATGCTGGGAGATTACATCTT  120

Query  310  CTCTATGGCAAGCGTGACTTCTTGCTGAGTGACAAAGCCTCTAGCCTCCTCTGCTTCCAG  369
            ||||||||||||||||||||||||||||||||||||||||||||||||||||||||||||
Sbjct  121  CTCTATGGCAAGCGTGACTTCTTGCTGAGTGACAAAGCCTCTAGCCTCCTCTGCTTCCAG  180

Query  370  CACCAGGAGGAGAG  383
            ||||||||||||||
Sbjct  181  CACCAGGAGGAGAG  194
```

Figure B.2 Sequencing result of Y88C mutation on ADGRG1/GPR56. The box shows nucleotide change (263 A > G) on cDNA of the receptor.

Score	Expect	Identities	Gaps	Strand
353 bits(191)	1e-101	193/194(99%)	0/194(0%)	Plus/Plus

```
Query  190  GCCCTCACAGTCCATGCCCCTTTCCCTGCAGCCCACCCTGCTTCCCGATCCTTCCCTGAC  249
            ||||||||||||||||||||||||||||||||||||||||||||||||||||||||||||
Sbjct  1    GCCCTCACAGTCCATGCCCCTTTCCCTGCAGCCCACCCTGCTTCCCGATCCTTCCCTGAC  60

Query  250  CCCAGGGGCCTCTACCACTTCTGCCTCTACTGGAACCGACATGCTGGGAGATTACATCTT  309
            |||||||||||||||||||| ||||||||||||||||||||||||||||||||||||||
Sbjct  61   CCCAGGGGCCTCTACCACTTCTCCCTCTACTGGAACCGACATGCTGGGAGATTACATCTT  120

Query  310  CTCTATGGCAAGCGTGACTTCTTGCTGAGTGACAAAGCCTCTAGCCTCCTCTGCTTCCAG  369
            ||||||||||||||||||||||||||||||||||||||||||||||||||||||||||||
Sbjct  121  CTCTATGGCAAGCGTGACTTCTTGCTGAGTGACAAAGCCTCTAGCCTCCTCTGCTTCCAG  180

Query  370  CACCAGGAGGAGAG  383
            ||||||||||||||
Sbjct  181  CACCAGGAGGAGAG  194
```

Figure B.3 Sequencing result of C91S mutation on ADGRG1/GPR56. The box shows nucleotide change (272 G > C) on cDNA of the receptor.

Figure B.4 Sequencing result of C346S mutation on ADGRG1/GPR56. The box shows nucleotide change (1036 T > A) on cDNA of the receptor.

Figure B.5 Sequencing result of W349S mutation on ADGRG1/GPR56. The box shows nucleotide change (1046 G > C) on cDNA of the receptor.

Figure B.6 Sequencing result of R565W mutation on ADGRG1/GPR56. The box shows nucleotide change (1693 C >T) on cDNA of the receptor.

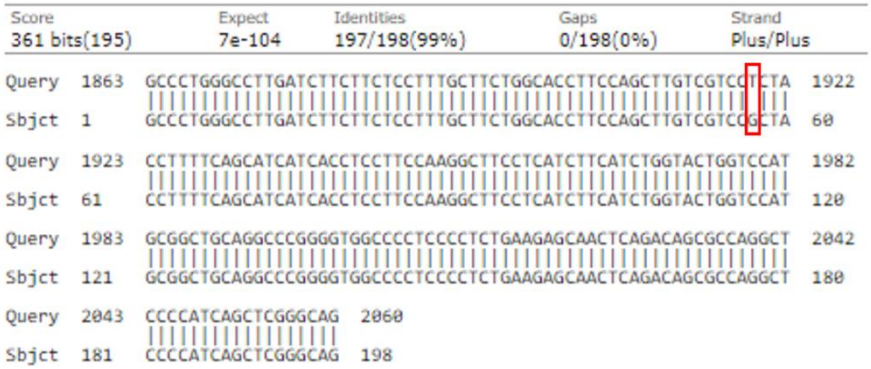

Figure B.7 Sequencing result of L640R mutation on ADGRG1/GPR56. The box shows nucleotide change (1919 T > G) on cDNA of the receptor.

C. Bacterial Cell Culture

Luria-Bertani (LB) broth

Table C.1 Luria-Bertani broth ingredients (for 1 L).

Component	Amount
Tryptone	10 g
Yeast Extract	5 g
NaCl	10g

After dissolving the ingredients above, 20 g of agar is added to the mixture and autoclaved. After that, ampicillin is added to the mixture in 1:1000 ratio under sterile conditions.

Super Optimum Broth with catabolite repression (SOC)

Table C.2 SOC ingredients (for 1 L).

Component	Amount
Tryptone	20 g
Yeast Extract	5g
1M Na Cl	10 mL
1M KCl	2,5 mL
autoclave and add below ingredients	
1M $MgCl_2.6H_2O$, 1M $MgSO_4.7H_2O$	10 mL
2M glucose	10 mL

D. Western Blot

Radioimmunoprecipitation assay (RIPA) buffer

Table D. 1 5x RIPA buffer ingredient (for 20 mL).

Component	Amount
1M Tris-HCl, pH 8.0	5 mL
1M NaCl	1,5 mL
NP-40	1 mL
SDS	0,1 g
Sodium deoxycholate	0,5 g

The buffer is sterilized by using 0.22 µm pore sized filter. Before using the buffer, protease inhbitors are added as shown below:

Table D. 2 Protease inhibitors added RIPA buffer (for 5 mL).

Components	Amount
5x RIPA	1 mL
1M DTT	5µL
100 mM PMSF	25 µL
1M Na β-glycerophosphate	250 µL
cOmplete™ ULTRA Tablets, Mini, EDTA-fee, EASYpack Protease Inhibitor Cocktail (Roche, Switzerland)	1/2

Laemmli (Sample) buffer

Component	Amount
SDS	0,8 g
1M Tris-HCl, pH 6.8	2,5 mL
0.1% Bromophenol blue	0,8 mL
Glycerol	4 mL
0.5 M EDTA	0.5 mL
β-mercaptoethanol	2 mL

Running Buffer

Component	Amount
Tris-HCl	24 g
Tris-base	5,6 g
NaCl	88 g

E. Tris-Buffered saline (TBS)

Component	Amount
Tris-HCl	24 g
Tris-base	5,6 g
NaCl	88 g
H2O	800 mL

F. Tris-Buffered saline with Tween (TBST)

Component	Amount
TBS	250 mL
Tween	250 µL

G. BRET Buffer

Table E.1 BRET buffer ingredients (for 1 L).

Component	Amount
0.1% Glucose	1 g
1M MgCl2	500 µL
10x PBS	100 mL

The buffer is sterilized by using 0.22 µm pore sized filter.

Note: All buffers are completed to indicated volumes (1L) by using MiliQ water.